Geophys. J. Int. (2004) **157,** 1331–1347 doi: 10.1111/j.1365-246X.2004.02261.x

Earthquake recurrence parameters from seismic and geodetic strain rates in the eastern Mediterranean

Sarah Jenny,[1,2] Saskia Goes,[1] Domenico Giardini[1] and Hans-Gert Kahle[2]

[1] *Institute of Geophysics, Swiss Federal Institute of Technology, Zurich, Switzerland. E-mail: sarah@tomo.ig.erdw.ethz.ch*
[2] *Geodesy and Geodynamics Lab, Swiss Federal Institute of Technology, Zurich, Switzerland*

Accepted 2004 January 28. Received 2004 January 14; in original form 2002 November 22

SUMMARY

Although the parameters used in seismic hazard analyses imply a long-term seismic strain rate, they are usually not checked against such alternative estimates. In this study, we determine hazard parameters for the eastern Mediterranean (a-value, b-value, $m_{\max}$ and the corresponding long-term seismic moment rate $\dot{M}_0^{\text{seis}}$) consistent with seismicity data, tectonic information and geodetic strain rates. The dense data coverage in this region permits a detailed comparison of the horizontal seismic strain rate field, $\dot{\varepsilon}_s$, as recorded in the 500-yr long historical catalogue and the tectonic strain rate field, $\dot{\varepsilon}_g$, measured geodetically. We find that $\dot{\varepsilon}_s$ is very similar in style over all magnitude ranges within each different tectonic regime in the study region. Furthermore, $\dot{\varepsilon}_s$ is similar in style to $\dot{\varepsilon}_g$. Except along the Hellenic Arc, $\dot{\varepsilon}_s$ is consistent with $\dot{\varepsilon}_g$ in amplitude. We verify that for the high strain rates accommodated in the eastern Mediterranean and historical catalogues spanning at least 100–200 yr, $\dot{\varepsilon}_s$ should reflect the long-term seismic strain release when averaged over each tectonic zone. To estimate such seismic strain reliably, accurate knowledge about the rates of recurrence of intermediate size events ($M_w = 4.5$–6.5) is needed. For $b \geq 1$, these events can accommodate up to 60 per cent of the strain. The combined analysis of $\dot{\varepsilon}_g$ and $\dot{\varepsilon}_s$ provides an estimate of the seismic/total strain. The major strike-slip zones in the region, the Northern Anatolian Fault and the Kephalonian Fault, experience little to negligible aseismic deformation. In the remaining eastern Mediterranean up to 10–30 per cent of the total deformation is aseismic. The Hellenic Trench is largely uncoupled, with at least 50 per cent and up to 90 per cent of the compressive strain released aseismically. Only the extensional component of strain at the eastern end of this trench appears significantly seismically active.

Key words: b-values, geodesy, seismic-event rates, seismicity, seismic moment.

1 INTRODUCTION

Knowledge of long-term seismic strain rates is essential for determining the seismic hazard of a region. Probabilistic seismic hazard analyses make an implicit estimate of long-term seismic strain rates. In hazard studies, the region of interest is divided into seismic source zones in which seismicity is assumed to be homogeneously distributed. For each source zone a magnitude–frequency seismicity distribution is determined, usually in terms of a Gutenberg–Richter relation and a maximum magnitude. The integrated moment rate of this distribution is equivalent to a seismic strain rate estimate. However, the strain rate fields implied by the seismic hazard data are generally not checked against other strain rate data. For example, for some regions, the hazard parameters from the Global Seismic Hazard Assessment Programme (GSHAP) (Giardini & Basham 1993; Giardini 1999) yield tectonically unrealistic strain rates that exceed geodetically inferred strain rates by a factor of 2–10. Although unrealistic strain rates do not necessarily lead to unreliable short-term hazard maps, it is preferable to use a set of hazard parameters that is consistent with all available data. The objective of this study is to evaluate how different sources of data can be used and integrated for this purpose.

Our study focuses on the eastern Mediterranean. First, we determine the geodetic and seismic strain rate fields for the region independently. By comparing these two fields we estimate long-term seismic strain rates, where long-term is defined as encompassing many large-earthquake cycles. Then we translate strain rates into earthquake recurrence parameters as used in hazard analyses. The dense geodetic data distribution, relatively long historical catalogues and high activity rates make this region ideal for constructing independent estimates of seismic and geodetic strain rates. Once the strengths and weaknesses of the individual data sources are known, future applications to regions with less dense data coverage become feasible.

Geodetic and seismic strain rates are mapped using the method of Haines & Holt (1993), which allows the determination of strain rate fields and corresponding velocity fields within a zone of continuous deformation by integrating seismic, geodetic and geological

information. Using the latest GPS measurements (Davies *et al.* 1997; Reilinger *et al.* 1997; Clarke *et al.* 1998; Cocard *et al.* 1999; McClusky *et al.* 2000; Kotzev *et al.* 2001), we are able to map geodetic strain rates in more detail than done in previously proposed deformation models for the eastern Mediterranean (Makris 1978; McKenzie 1978; Le Pichon & Angelier 1979; Le Pichon *et al.* 1995; Giunchi *et al.* 1996; Mantovani *et al.* 2000). The data we use exclude short-term co- and post-seismic deformation (Cocard *et al.* 1999; McClusky *et al.* 2000). On a global scale, it has been demonstrated that geodetic strain rates and tectonic deformation rates inferred from geology agree well (for example Ward 1990; DeMets *et al.* 1994; Argus & Heflin 1995). A similar agreement has been found along the western and eastern parts of the North Anatolian Fault Zone (NAFZ) (Armijo *et al.* 1999; Straub *et al.* 1997; Westaway 1994). Therefore, we take the geodetic strain rate field as representative for long-term tectonic deformation.

To define a seismic strain rate field, the style is obtained from moment tensors, using Kostrov summation, while the magnitude is inferred from historical catalogues going back to 500 BC. Others have performed analyses of seismic deformation rates using around 100 yr of historical seismic data (Jackson & McKenzie 1988; Jackson *et al.* 1992). Papazachos & Kiratzi (1992) combined historical data back to the 18th century and moment tensors within a study area in central Greece. We map seismic strain rates on the same grid as used for the geodetic field, and evaluate uncertainties due to uncertainties in mechanism, magnitude and completeness. The main factors that contribute to uncertainties in estimates of long-term seismic moment rate from historical catalogues have been analysed in detail by Field *et al.* (1999).

We compare geodetic and seismic strain rates to obtain an estimate of long-term seismic moment rates. Such moment rates should neither exceed tectonic moment rates nor require events of unreasonably large magnitude. Seismic moment rates that are low compared with tectonic strain rates may indicate that deformation occurs in part aseismically (or in other words, that the depth of seismic coupling varies). Using the observed magnitude–frequency distributions of seismicity and their uncertainties, we translate the seismic moment rates into earthquake recurrence parameters for the simple truncated Gutenberg–Richter distribution often used in hazard analyses. Ward (1998a) has previously estimated and compared seismic and geodetic moment rates in Europe for a less dense geodetic data set and using the seismicity of the 20th century from the NEIC catalogue. He found that, overall, the seismic moment rates are less than geodetic moment rates. This, however, does not imply significant aseismic deformation, as short catalogues are more likely to underestimate than overestimate long-term moment rates (Ward 1998a,b). Jackson *et al.* (1994) compared seismic and geodetic strains in the Aegean. The distribution of geodetic data at the time allowed only a coarse grid study. They found a seismic strain rate deficit for the whole Aegean area. Recently, Koravos *et al.* (2003) performed a significantly more detailed study of the seismicity distribution and moment release rates in the Aegean. To obtain maximum magnitude estimates they relied on the geodetic strain of Jackson *et al.* (1994). In the analysis done here, we update both seismic and geodetic deformation fields and compare them in style as well as in amplitude.

2 TECTONIC SETTING OF THE EASTERN MEDITERRANEAN

The Aegean–Anatolian region is an area of intense seismic activity relative to the surrounding areas. The region can be divided into five different tectonic regimes: (1) strike-slip motion along the NAFZ and its extension into the northern Aegean, the North Aegean Trough (NAT); (2) extension in central Greece, including the Gulf of Corinth and Peleponesos; (3) extension in western Anatolia; (4) convergence along the Hellenic Arc and (5) the Kephalonian Transform Fault (Fig. 1).

The NAFZ accommodates right-lateral strike-slip motion between Anatolia and stable Europe. Releasing steps in the fault form pull-apart basins in the Marmara Sea (Barka 1997). The westward extrusion of Anatolia is probably a response to Arabian indentation (Jackson & McKenzie 1988; Le Pichon *et al.* 1995). The NAFZ is a relatively recent tectonic feature of the region. It formed around 10 Mya in eastern Turkey (Barka 1992) and propagated westward (Taymaz *et al.* 1991b; Armijo *et al.* 1999). At present, the fault zone extends into the NAT where several linear trends of strike-slip earthquakes can be discerned. This strike-slip motion is transferred into normal faulting (with the direction of the principal extension being constant) in continental Greece (Hatzfeld *et al.* 1999). Slip rates along the NAFZ have been estimated by seismic moment summation (Jackson & McKenzie 1988; Eyidoğan 1988; Kiratzi 1993; Westaway 1994), geological information (Barka & Kandinsky-Cade 1988; Taymaz *et al.* 1991a; Lyberis *et al.* 1992) and geodetic velocities (Straub *et al.* 1997; McClusky *et al.* 2000). The velocities obtained by recent GPS campaigns constrain the rates of the westward motion of the Anatolian Plate along the NAFZ to 26 ± 3 mm yr^{-1} relative to Eurasia.

North–south directed extension is currently localized in central Greece, around the Gulf of Corinth and the regions north and south of it (Sorel 2000). Around 25–30 Mya extension occurred further south and in the Aegean Sea (Jolivet *et al.* 1994; Gautier *et al.* 1999). The southern Aegean is at present seismically very quiet and is often treated as a rigid block. Some extension is also observed in western Anatolia, but it is less pronounced geodetically (Jackson & McKenzie 1984; Seyitoglu & Scott 1996; Kahle *et al.* 1999). The extension in Greece and western Anatolia is probably a response to trench roll-back (Jolivet 2001).

Convergence along the Hellenic Arc is currently active from the Kephalonian Transform Fault in the northwest to Rhodes in the southeast. The trench is marked by recently deformed sediments and a high level of seismicity consisting predominantly of small events. Very few large thrust events have been documented and the level to which the subduction zone interface is coupled and, thus the seismic strain rate, is not well constrained (Jackson & McKenzie 1988; Meijer & Wortel 1997). The Hellenic Trench is also associated with active extension parallel to the arc (Lyon-Caen *et al.* 1988; Armijo *et al.* 1992).

The Kephalonian Fault marks the western termination of the active subduction at present. Active subduction north of Kephalonia ceased around 5 Mya (King *et al.* 1993; Robertson & Shallo 2000), and was replaced by continental collision between the Adriatic and the Balkans. The Kephalonian fault exhibits dextral strike-slip motion, at a rate of 2–3 cm yr^{-1}(Kahle *et al.* 1996; Cocard *et al.* 1999; Louvari *et al.* 1999).

3 STRAIN MAPPING METHOD

We treat deformation as continuous within the Aegean–Anatolian region. We use the method developed by Haines & Holt (1993), upgraded and discussed in more detail by Haines *et al.* (1998) and Beavan & Haines (2001), and applied in various regions (for example Holt & Haines 1995; Shen-Tu *et al.* 1999; Kreemer *et al.*

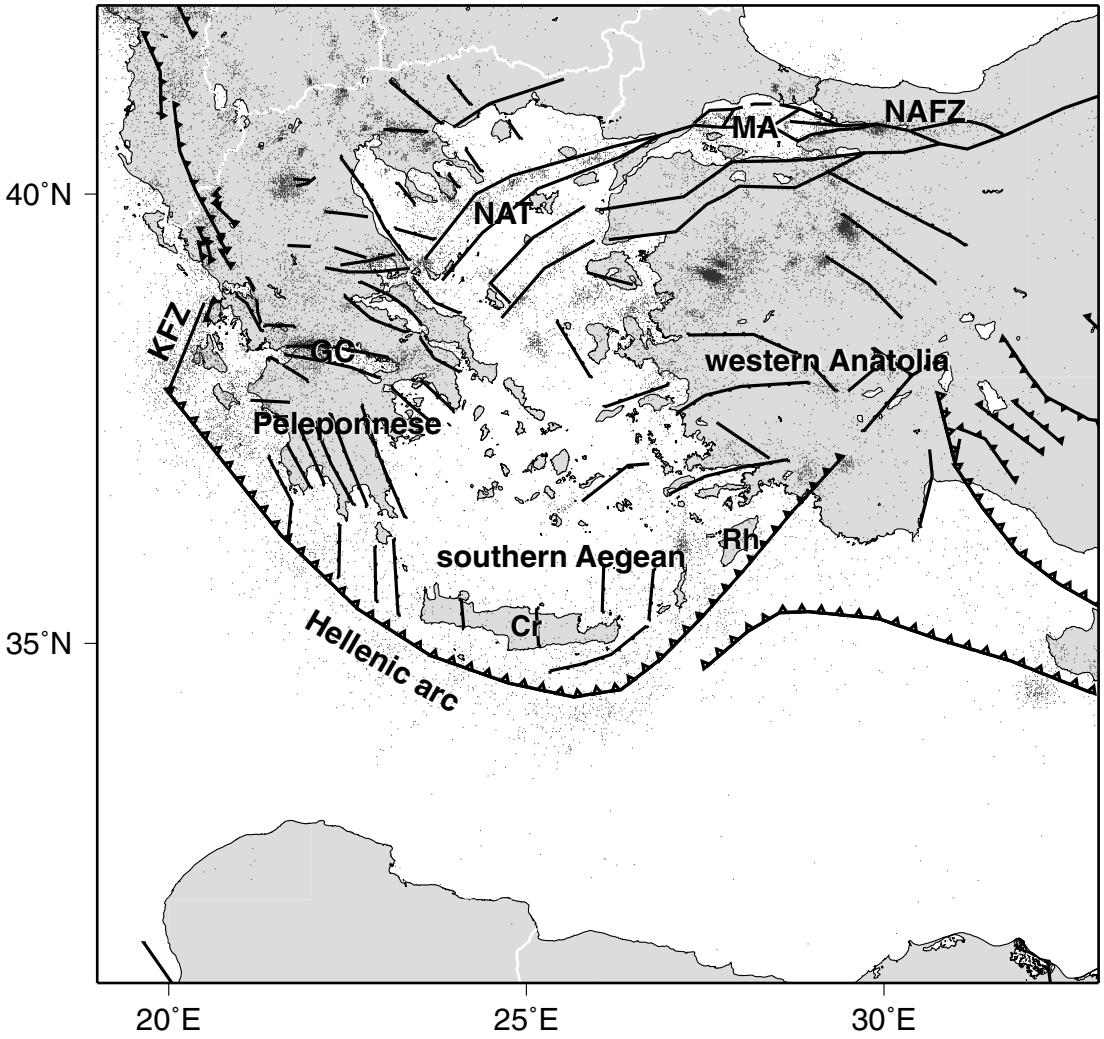

Figure 1. Tectonic setting of the study region showing major faults (after Kahle *et al.* 2000) and seismicity from the PDE-NEIC catalogue (US Geological Survey 1998) for depths ≤40 km and a time span of 1/1/1977–31/12/2001. Cr = Crete, GC = Gulf of Corinth, KFZ = Kephalonian Fault Zone, MA = Marmara Sea, NAFZ = North Anatolian Fault Zone, NAT = North Anatolian Trough, Rh = Rhodes.

2000). Haines & Holt (1993) show that velocity and strain rate on a sphere can be expressed in terms of the rotation vector function $\mathbf{W}(\hat{\mathbf{x}})$, which describes the velocity field $\mathbf{u}(\hat{x})$,

$$\mathbf{u}(\hat{x}) = r\mathbf{W}(\hat{x}) \times \hat{x}, \tag{1}$$

where $\hat{\mathbf{x}}$ is the unit radial position vector on the Earth's surface and r is the radius of the Earth. This method provides a consistent strain rate field (compatible and related to $\nabla\mathbf{u}(\hat{x})$) and allows for the combination and comparison of different data types (seismic, geodetic and geological). Their method determines $\mathbf{W}(\hat{\mathbf{x}})$ at the knot points of a curvilinear grid assuming a bi-cubic spline interpolation between the nodes to obtain a continuous $\mathbf{W}(\hat{\mathbf{x}})$ field that satisfies strain rate compatibility constraints. $\mathbf{W}(\hat{\mathbf{x}})$ at the nodes is obtained from a weighted least-squares minimization between observed and predicted values of velocity (in the case of geodetic data) and/or strain rate (in the case of seismic data). Weights are given by the estimated data covariance. Depending on the data distribution some smoothing over one to several neighbouring grid cells is usually required. In the case of seismic data, strain rates are estimated from Kostrov summation (Kostrov 1974):

$$\dot{\varepsilon}_{ij} = \frac{1}{2\mu V T} \sum M_0 \boldsymbol{m}_{ij} \tag{2}$$

where μ is the shear modulus, V is the cell volume (the grid area times the seismogenic thickness), T is the time period of the earthquake record, M_0 is the seismic moment, and $\boldsymbol{m}_{ij}$ is the unit moment tensor. We use a shear modulus of 3.5×10^{10} N m^{-2} and an average 15 km thickness of the seismogenic zone. Values of μ and seismogenic thickness affect the magnitude but not the style of the estimated strain rate tensors. To determine self-consistent strain rate fields associated with GPS observations, velocities are matched subject to the constraint of minimal strain rate magnitude. Covariances are taken directly from the geodetic data (Hollenstein *et al.* 2003).

The choice of the grid is important. It should be fine near major faults to allow for large spatial variations in strain, but coarser in areas where sparse data do not provide detailed constraints. It should follow tectonic features so that smoothing is performed consistently with tectonics. For Kostrov summation grid cells should delimit areas of homogeneous tectonic deformation. Based on the main tectonic domains, seismicity maps and moment tensor data, a curvilinear grid is defined across the eastern Mediterranean region,

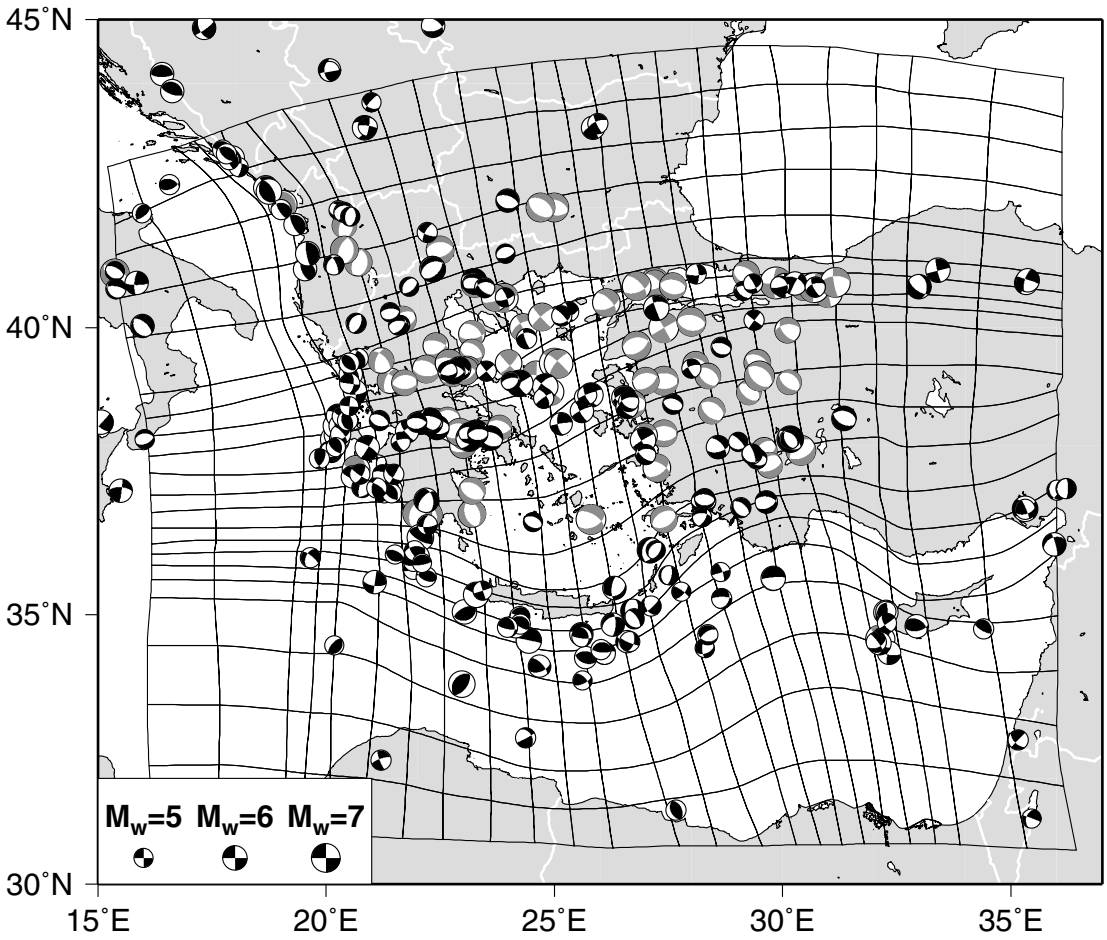

Figure 2. Focal mechanisms with $M \leq 6.5$ from the CMT catalogue in black (Dziewonski *et al.* 1981). Focal mechanisms with $M > 6.5$ from the Harvard CMT catalogue and from Jackson *et al.* (1992) in grey. All events have depths ≤40 km. Also shown is the grid on which Kostrov summation and strain rate mapping are performed.

covering an area between 13°and 36°E and between 30°and 47°N (Fig. 2).

Plate rigidity can be simulated by setting the spatial derivatives of $\mathbf{W}(\hat{\mathbf{x}})$ to zero. This is done for the part of the African Plate marked in (Fig. 3). The geodetic velocity field is calculated relative to a Eurasian reference frame. The northern boundary of the grid is kept fixed in this reference frame.

4 DATA

4.1 Seismic data

The style of seismic deformation within the Aegean–Anatolian region is derived from focal mechanism solutions of the Harvard Centroid Moment Tensor (CMT) catalogue (Dziewonski *et al.* 1981, http://www.seismology.harvard.edu) and a compilation of large events by Jackson *et al.* (1992) (Fig. 2). The CMT catalogue contains solutions for approximately all events with magnitude $M_w > 5.5$ since 1977 January; we use events up to 2003 August. Catalogues spanning the entire 20th century for the eastern Mediterranean have been compiled by Anderson & Jackson (1987), Jackson & McKenzie (1988) and Jackson *et al.* (1992), but contain only large events ($M \geq 6.0$) and have larger uncertainties. The mechanisms from the short CMT catalogue agree well with the data of Jackson *et al.* (1992). Most of the slight differences between the deformation styles in the two data sets disappear when the moment tensors are averaged. To obtain strain rate estimates, we include all events at depths less than 40 km, which reflect lithospheric deformation related to horizontal surface motions. Most of the events (90 per cent) are located above 15 km, the depth used in the Kostrov strain calculation, but to allow for depth uncertainties we set the depth cut-off to 40 km.

Historical catalogues provide information about moment rates over a much longer period and give constraints on the magnitude of the seismic strain rates. To assess uncertainties and improve the catalogues, we combine the results of several catalogues. The catalogue of Ambraseys & Jackson (2000) for the Marmara Sea contains all earthquakes between AD 1500 and 2000 with $M_s \geq 6.0$ and is believed to be complete above $M_s \geq 6.8$. Ambraseys (2001a) further compiled a catalogue for the time interval 1900–1999 in the eastern Mediterranean including Greece and the Middle East for shallow earthquakes ($h \leq 40$ km) with $M_s \geq 6.0$. Seismicity in Greece west of 30°E for the period 550 BC to AD 1999 is available from Papazachos *et al.* (2000). For Turkey a declustered catalogue has been prepared for the Global Seismic Hazard Assessment Programme (GSHAP) (Giardini 1999, http://seismo.ethz.ch/GSHAP/turkey/seisgshap.prn). Finally the NEIC-PDE catalogue (US Geological Survey 1998), although

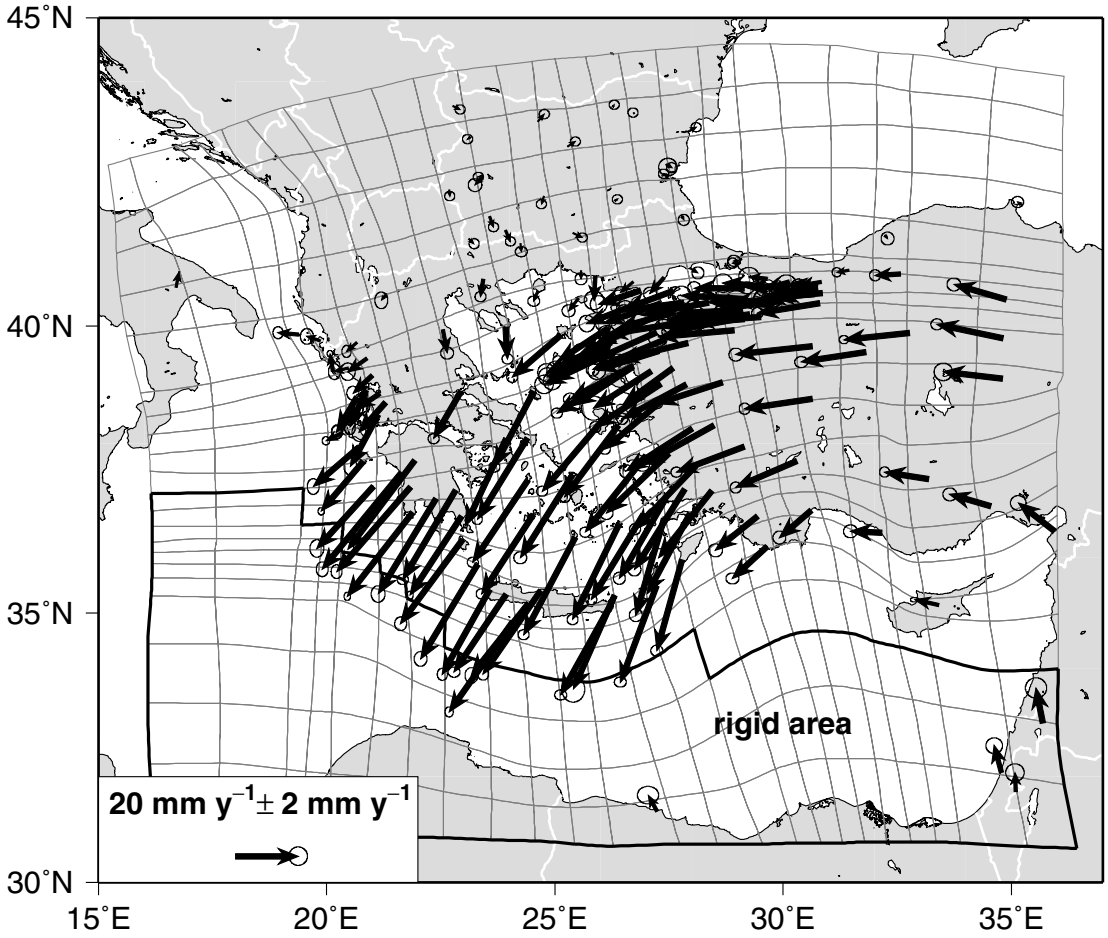

Figure 3. GPS velocities relative to Eurasia used in the inversion. Data are from (1) Kotzev *et al.* (2001) for the period 1996–1998 in Bulgaria, (2) McClusky *et al.* (2000) for the period 1988–1997 at sites within Greece and eastern Turkey and (3) Cocard *et al.* (1999) for the period 1993–1998 across the west Hellenic Arc. The black line delimits the rigid African Plate which is moving according to the rotation pole of Fernandes *et al.* (2003).

short, contains a considerable number of small events for the time span 1973 to present which allows the mapping of tectonic features that are moving seismically (Fig. 1). These different sources were merged and carefully cross-checked to produce our own historical catalogues. The magnitude and location of events are not always in agreement amongst the various authors. To assess the impact of these uncertainties on the determination of the moment rates and the earthquake recurrence parameters, we define two catalogues. Both catalogues comprise the catalogue of Papazachos *et al.* (2000) west of 30°E and the the GSHAP-Turkey and the NEIC-PDE catalogues east of 30°E. The first one, CAT1, spans only the last 500 yr, and where available the data of Ambraseys & Jackson (2000) and Ambraseys (2001a) for events larger than $M_w = 6$ are used instead of those of Papazachos *et al.* (2000) and GSHAP. The second catalogue, CAT2, spans the full 2550 yr, and the data were not modified from Papazachos *et al.* (2000) and GSHAP. To assess the effects of uncertain completeness intervals, we use published estimates (Papazachos 1999; Papazachos *et al.* 2000) west of 30°E, as well as our own estimates (Table 1) based on the method of Mulargia *et al.* (1987) that identifies changes in seismicity rate. The same range of completeness intervals is used for CAT1 and CAT2.

The other large sources of uncertainty are the earthquake magnitudes. The magnitude reported by Papazachos *et al.* (2000) is an equivalent moment magnitude, calculated by relations that transfer magnitudes of locally used scales to moment magnitudes M_w (Papazachos *et al.* 1997). Papazachos *et al.* (2002) showed that these equivalent magnitudes are practically equal to M_w, with an overall standard error $\sigma = 0.23$. The catalogues of Ambraseys & Jackson (2000) and Ambraseys (2001a) use M_s, which is similar to M_w in the range $5.0 \leq M_s \leq 7.5$ (Hanks & Kanamori 1979). The GSHAP catalogue lists M_w. In their study of the Aegean region, Koravos *et al.* (2003) used only the catalogue of Papazachos *et al.* (2000). They revised the magnitudes of all events before 1904 down by 0.4. This revision is based on the probable magnitude overestimate of two large events for which alternative data are available (Abe & Noguchi 1983; Ambraseys 2001b). Rather than applying a systematic shift, we prefer to use two catalogue alternatives, where it should be noted that many of the magnitudes of Ambraseys & Jackson (2000) and Ambraseys (2001a) (including those of the two afore mentioned events) are lower than those in CAT2. In addition, we assign the following magnitude errors (Papazachos *et al.* 2000): $\pm$ 0.25 for the instrumental period (1911–2000), $\pm$0.35 for the historical period (1500–1911) and $\pm$ 0.5 for data prior to 1500. Errors in magnitude due to the approximation $M_s = M_w$ are included in these errors. Magnitude and completeness uncertainties are propagated through our analyses.

Table 1. The two combined historical seismic catalogues and the corresponding completeness length used in this study. Completeness intervals are in bold type, alternative completeness intervals are in italic type. Sources: 1, Ambraseys (2001a); 2, Ambraseys & Jackson (2000); 3, Papazachos *et al.* (2000); 4, GSHAP-Turkey; 5, NEIC-PDE. The sources are listed in order of priority.

Date	M_w range	500-yr catalogue CAT1	2550-yr catalogue CAT2
For area west of 30°E:			
≥ −**550**/*0–1499*	≥8.0		3
≥**1500**/*1600–1844*	≥7.3	1,2,3	3
≥**1845**/*1750–1899*	≥6.5	1,2,3	3
≥**1900**/*1845–1910*	≥6.0	1	3
≥**1911**/*1900–1949*	≥5.5	3	3
≥**1950**/*1911–1969*	≥5.0	3	3
≥**1970**	≥4.5	3	3
For area east of 30°E:			
≥**1500**/*1800–1844*	≥7.3	1,4	1,4
≥**1845**/*1900–1899*	≥6.5	1,4	1,4
≥**1900**/*1925–1924*	≥6.0	1.4	1.4
≥**1925**/*1950–1972*	≥5.5	4,5	4,5
≥**1973**/*1980–1999*	≥4.5	5	5

4.2 Geodetic data

The GPS measurements of crustal motions we use are from McClusky *et al.* (2000), Cocard *et al.* (1999) and Kotzev *et al.* (2001). McClusky *et al.* (2000) compiled geodetic velocities for the period 1988–1997 at sites extending from the Caucasus mountains to the Adriatic Sea and from the southern edge of the Eurasian Plate to the northern edge of the African Plate. Cocard *et al.* (1999) carried out repeated GPS measurements in the period from 1993 to 1998 across the entire West Hellenic Arc. Kotzev *et al.* (2001) measured a regional GPS network in Bulgaria over the period 1996 to 1998. Fig. 3 shows the GPS velocities relative to Eurasia. For the motion of the rigid African Plate, we used the recent AFR–EUR rotation pole at −10.88° N, −16.16° E with a rate of 0.066° Myr^{-1} (Fernandes *et al.* 2003). This pole results in a NNW velocity for northeastern Africa and is based on a combination of geodetic observations. The velocities are significantly less than in NUVEL-1A. The necessity for lower AFR–EUR convergence velocities has been previously noted (Westaway 1990; Sella *et al.* 2002; Kreemer *et al.* 2003).

5 STRAIN RATE STYLE

5.1 Seismic

Although focal mechanisms from a few decades might not be expected to yield a reliable estimate of long-term seismic strain styles, Amelung & King (1997) found a very good agreement between seismic strain patterns inferred from earthquakes over several units of magnitude and regional tectonic strain patterns for the strike-slip regime of the San Andreas Fault in California. The results of Kreemer *et al.* (2000) for various tectonic regimes in Indonesia also showed gross agreement in deformation patterns over several units of magnitude, but differences in detail. Our study region also contains tectonic regimes other than strike-slip faulting. Therefore, we test the similarity of strain rate patterns of the seismic data over different magnitude ranges and compare these patterns with those of, presumably long-term tectonic, strain inferred from the GPS data.

The strain rates are determined by summing the moment tensors plotted in Fig. 2 within each cell of the curvilinear grid. The obtained moment tensors are smoothed over one neighbouring cell to obtain a strain rate field for most of the grid, that is, where no focal mechanisms are also available. Fig. 4(a) shows the direction only of the principal strain rate axes inferred by summing events up to $M_w = 5.9$ and up to $M_w = 6.5$ from the CMT catalogue. Similarly, Fig. 4(b) shows the direction of the principal strain rates axis inferred by summing events up to $M_w = 6.5$ and larger events of the CMT catalogue and from the catalogue of Jackson *et al.* (1992) which contains events up to $M_w = 7.6$. A similar style of deformation is observed for earthquakes in all magnitude ranges, for most of the study area. Note that differences between the principal axes of less than about 20°are within the uncertainties in the CMT solutions. Uncertainties in the older mechanisms are likely to be somewhat larger. Most of the small differences are due to smoothing into areas with poor data coverage (for example, the eastern Hellenic Arc and southwestern Turkey, around Crete, and the southern part of the Peleponesos; compare with Fig. 2). Given the overall consistency of the strain fields from larger and smaller events and because of the better quality and uniformity of the CMT catalogue, we use the events with $M_w \leq 6.5$ to define our best estimate of the style (not the magnitude) of the seismic strain rate field.

5.2 Geodetic

Using the method of Haines & Holt (1993), the geodetic velocities (Fig. 3) are inverted for a horizontal strain rate field. The principal axes of the geodetic strain are very similar in direction to the pattern of seismic strain (Fig. 5). Again, some differences are due to (different) smoothing of the seismic and/or geodetic strain rate field into areas of low data coverage (for example central Turkey and central Greece for the GPS data). Note that along the eastern part of the Hellenic Arc the compressional part of the geodetic strain rates perpendicular to the arc is almost absent in the seismic strain rates. In areas where seismic and geodetic strain rate fields reflect the same style of deformation, these data can be combined to constrain earthquake recurrence rates (Section 7).

6 STRAIN RATE MAGNITUDE

6.1 Seismic, from the catalogues

The moments of the events in our seismic catalogue CAT1 are summed within each grid cell, and converted into rates by dividing over the appropriate completeness interval for each magnitude range (Table 1: in bold). Only events with $M_w \geq 4.5$ are taken into account. If, as with most geodetic data sets, the vertical strain rate is unknown, the moment rate associated with a best-fitting double couple cannot be defined unambiguously. If also the predominant faulting style in the region is not known, Savage & Simpson (1997) propose to estimate scalar moment rates from horizontal strain rates as follows:

$$\dot{M}_0 = 2\mu V \mathrm{Max}(|\dot{\epsilon}_1|, |\dot{\epsilon}_2|, |\dot{\epsilon}_1 + \dot{\epsilon}_2|) \quad (3)$$

where μ is the shear modulus, V is the volume of the seismogenic zone and $\dot{\epsilon}_1$ and $\dot{\epsilon}_2$ are the principal horizontal strain rate axes. Although the seismic moment tensors do provide faulting style in most of the study area, moment rates are converted into horizontal strain rates using eq. (3) for consistency with the treatment of the geodetic strain rates. Fig. 6 shows the principal horizontal axes of the total seismic strain rate tensor obtained by combining the historic seismic moment rates of CAT1 with the styles from the $M_w \leq 6.5$

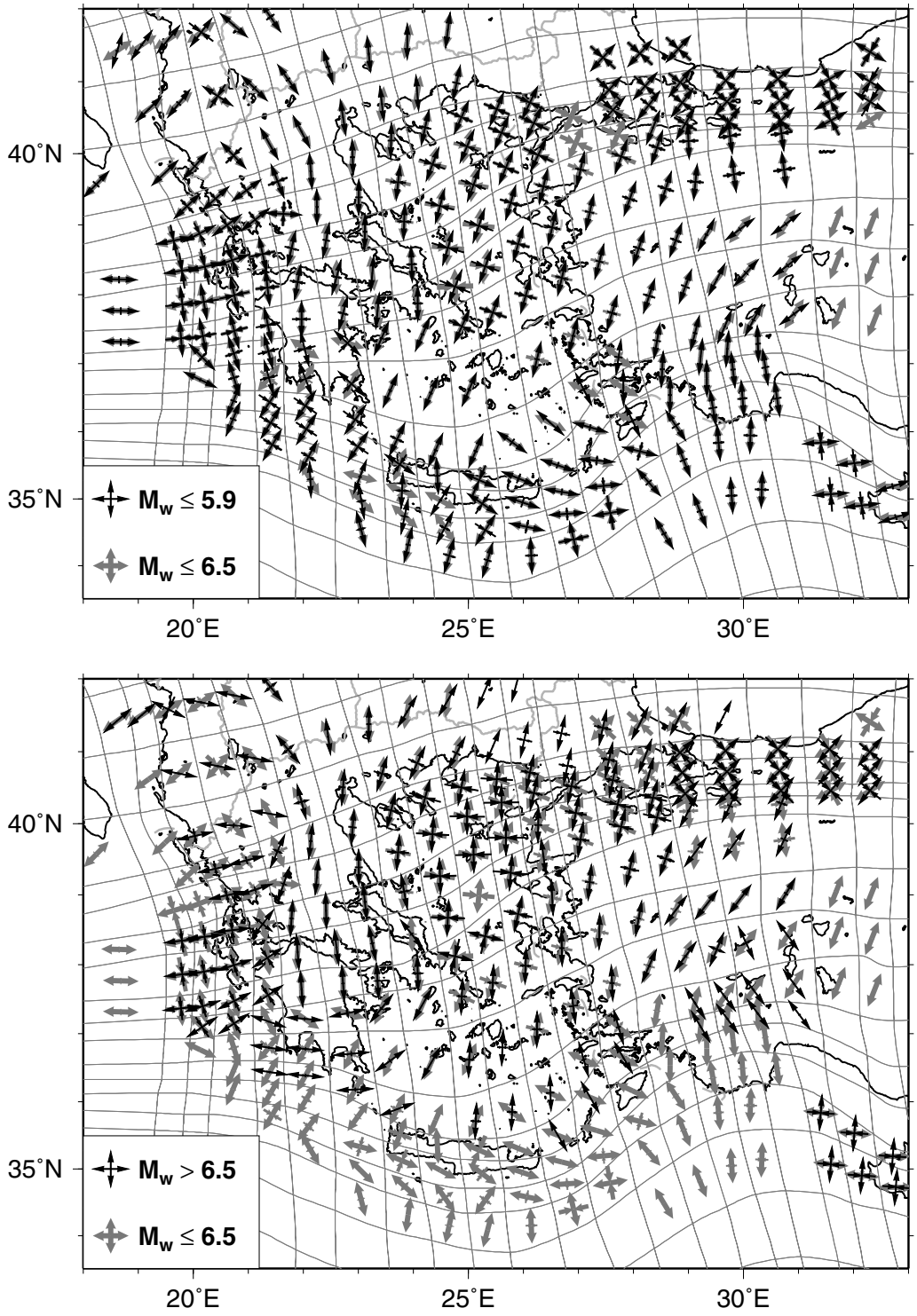

Figure 4. Style of the seismic strain rate field. (a) Direction of the principal strain rate axes of the unit moment tensors inferred by summing events up to $M_w = 5.9$ (in black) and up to $M_w = 6.5$ (in grey) of the CMT catalogue. (b) Direction of the principal strain rate axes of the unit moment tensors inferred by summing events up to $M_w = 6.5$ of the CMT catalogue (in grey) and larger events of the CMT and Jackson *et al.* (1992) (in black). The direction of the principal strain rate axes is consistent over a large range of magnitudes.

events of the CMT catalogue (Fig. 4). Note that only the strain rate styles are smoothed over one neighbouring grid cell; the moment rate magnitudes are unsmoothed.

The largest strain rates are found (1) along the NAFZ east of the Marmara Sea, (2) in the NAT, along the continuation of the NAFZ, (3) within the eastern part of the Gulf of Corinth and just NE of it, (4) along the Kephalonian Fault, and (5) along the Hellenic Arc especially along the eastern part. Although the strain rate field is dominated by larger events ($M_w \geq 7.0$), high strain rates also correlate with high seismicity rates, and smaller events in the range

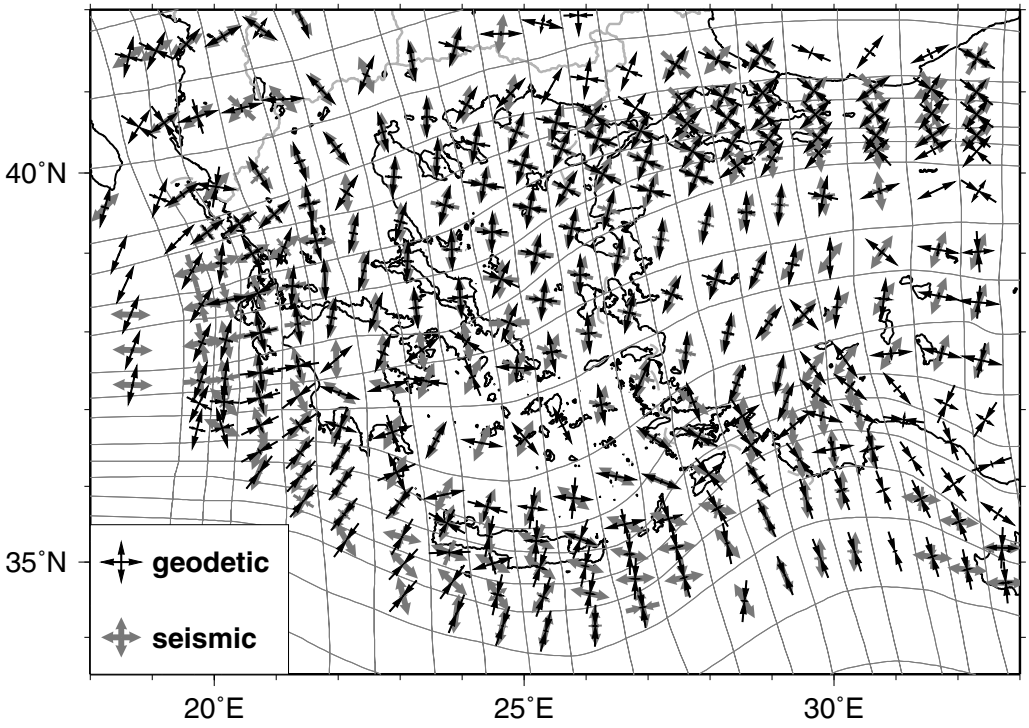

Figure 5. Comparison of the direction of the principal strain rate axes of the unit moment tensors inferred by summing events of the CMT catalogue up to $M_w = 6.5$ (in grey) and obtained by the inversion of GPS data in Fig. 3 (in black).

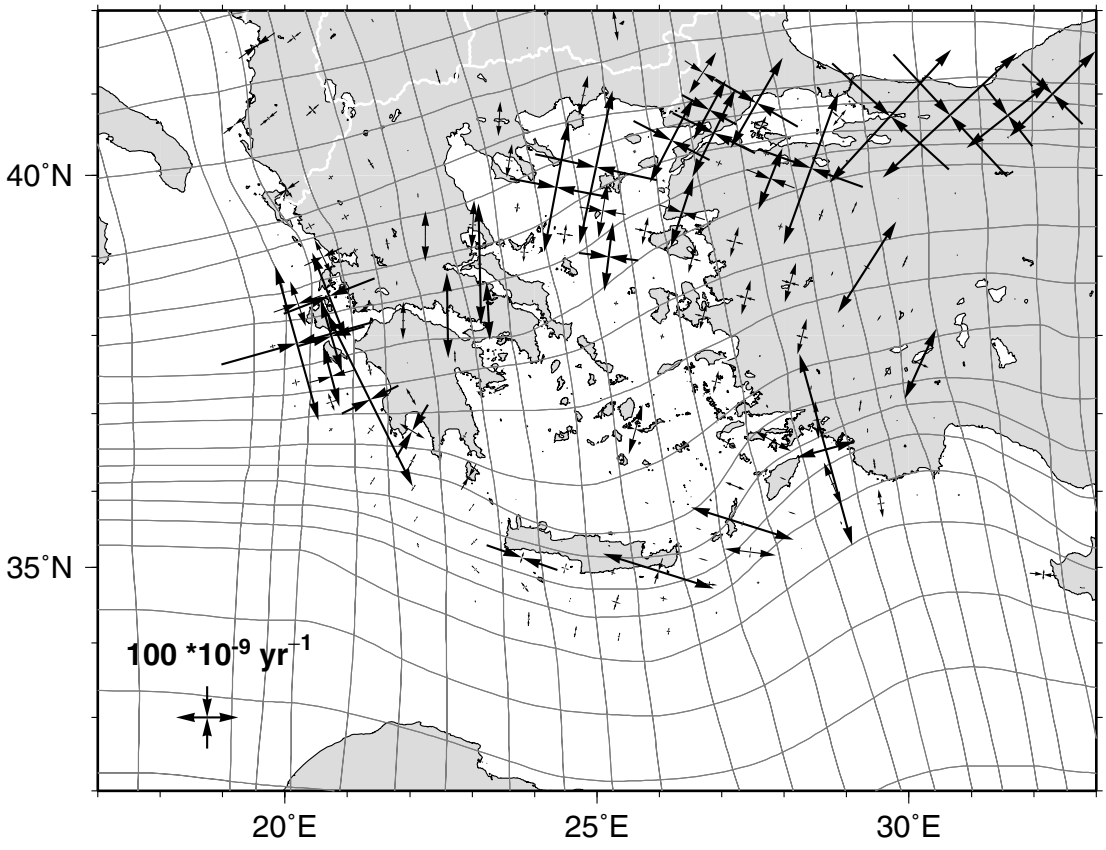

Figure 6. Principal horizontal axes of the total seismic strain rate tensor obtained by combining the seismic moment rates of the 500-yr catalogue (CAT1) with the styles inferred from the $M_w \leq 6.5$ events of the CMT catalogue.

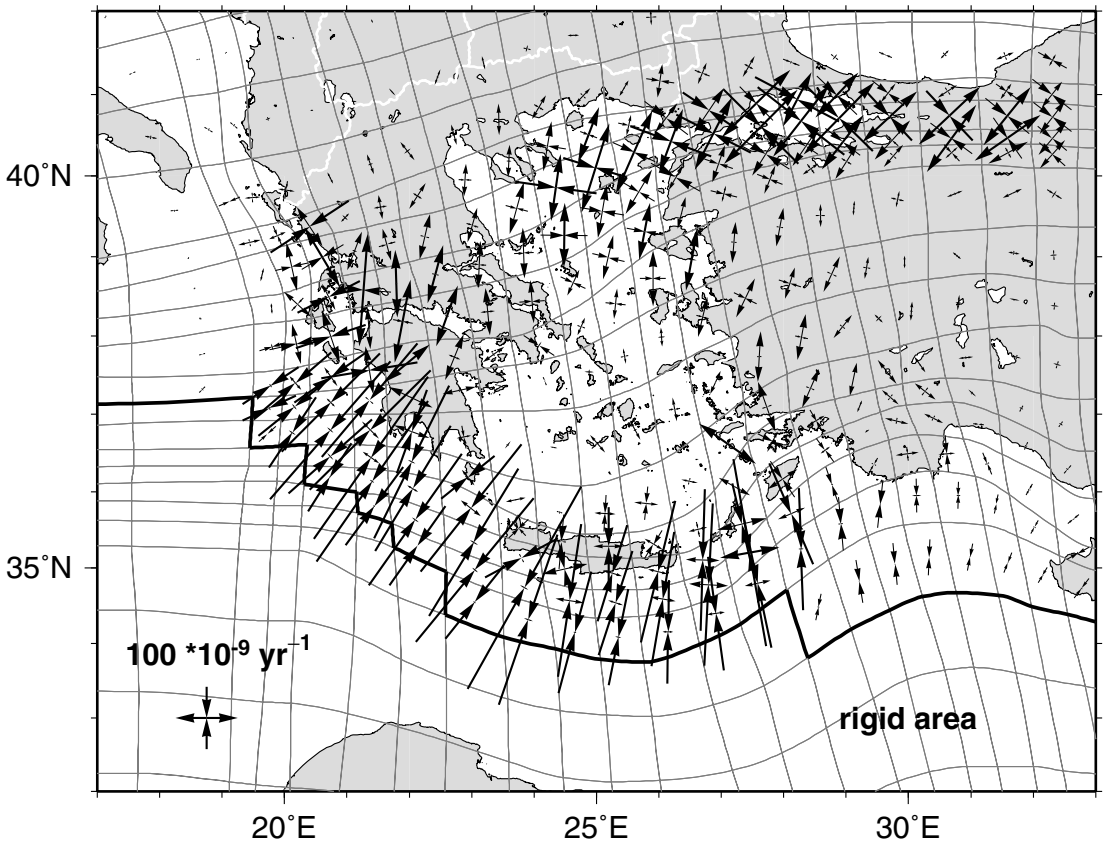

Figure 7. Principal horizontal axes of the total geodetic strain rate field obtained with the method of Haines & Holt (1993) from fitting the GPS velocities plotted in Fig. 3.

$M_w = 4.5$ –6.5 contributed up to 60 per cent of the total seismic moment rate in certain areas. Note that data in southwestern Turkey are sparse and the quality of the seismicity data here is poorer than in the rest of our study area.

The uncertainty in moment rates due to uncertainties in magnitude, location and completeness of the catalogues is estimated by comparing our two catalogues, CAT1 and CAT2, along the NAFZ where the data in the catalogues differ the most. This yields a variation of up to a factor of 2 in moment rates. Similar uncertainties probably exist in other regions as well and an uncertainty of a factor of 2 is assigned to the whole study area. The seismic moment rates are scaled to strain rates with a constant seismogenic thickness of 15 km, which is a reasonable estimate of the depth range over which the bulk of the seismic strain is accommodated in continental areas. Different values of μ times the seismogenic thickness lead to a change of up to 30–40 per cent in the moment rates, that is, much less than the effect of catalogue uncertainties. At the trench, the effective seismogenic thickness may be twice as large, which would reduce the estimated seismic strain rates by a factor of 2.

6.2 Tectonic, from GPS data

The principal horizontal axes of the total geodetic strain rate field are shown in Fig. 7 on the same scale as the seismic strain rates in Fig. 6. The strain rate field is consistent with the fields obtained with similar data but different methods (Kahle *et al.* 2000; Nyst 2001). The geodetic deformation field (Fig. 7) is dominated by one broad band of right-lateral strike-slip deformation along the NAFZ and its prolongation in the Aegean, extension around the Gulf of Corinth, and strike-slip in the area of the Kephalonian Fault. These regions coincide with the regions of the highest seismic strain rates (Fig. 6). In addition, a strong component of compression is found in the geodetic strain rates along most of the Hellenic Arc which is absent in the seismic strain rates. The concentration of strain along the arc is dictated by the constraint of a rigid African Plate, just south of the trench. We defined the extent of the rigid African Plate based on the seismicity. Although some deformation and seismicity occur south of the trench in the Mediterranean Ridge accretionary complex (Kreemer & Chamot-Rooke 2004), most seismicity is located near the trench, and we assume that, for the 15 km depth interval considered, the trench accommodates the Aegean-African convergence of around 4 cm yr^{-1}.

The geodetic strain rate field is much smoother than the seismic strain rate field. In part this is the result of smoothing induced by the bi-cubic spline approximation in the inversion of geodetic data, where the seismic strain rates were smoothed only in style. But largely it reflects the differing characters of long-term tectonic and short-term seismic strain rates. The geodetic data measure both distributed (short-term) elastic loading and concentrated permanent deformation (seismic as well as aseismic) which, when averaged over length scales exceeding those of elastic loading, add up to long-term tectonic rates. By contrast, the seismicity reflects permanent, seismic, strain only, measured over the duration of a catalogue that is generally less than several earthquake recurrence cycles. A useful comparison of geodetic (that is, tectonic) strain rates and seismic catalogue strain rates can only be made on scales that exceed the

Table 2. Terminology.

	seis	cat	tec
$\dot{M}_0$	Estimated long-term seismic moment rate	Moment rate obtained from catalogue	Geodetically estimated $\dot{M}_0$
$m_{\max}$	Estimated long-term max. magnitude	Largest event size in the catalogue	Max. magnitude required to give $\dot{M}_0^{\text{seis}} = \dot{M}_0^{\text{tec}}$
$a_1, b_1, m_{\max}^1$:	$b_1 = 1, m_{\max}^1 = m_{\max}^{\text{cat}}$		$\Rightarrow a_1 =$ max. estimate of a
$a_2, b_2, m_{\max}^2$:	a_2 : max. likelihood for $m_w = 4.5$ –6, $b_2 = 1$		$\Rightarrow m_{\max}^2$
$a_3, b_3, m_{\max}^3$:	a_3 and b_3 : max. likelihood for $M_w = 4.5 - m_{\max}^{\text{cat}}$		$\Rightarrow m_{\max}^3$

intrinsic (elastic) and applied smoothing of the geodetic deformation field. Such a comparison is made in the next section.

7 ESTIMATING EARTHQUAKE RECURRENCE PARAMETERS

The seismic and geodetic strain rates together with seismic magnitude–frequency data are used to define, for a set of source zones, the three parameters a, b and $m_{\max}$ of the truncated Gutenberg–Richter distribution commonly used in hazard analyses. The a-value is the recurrence rate of small events, the b-value describes the decrease in recurrence frequency with increasing magnitude, and $m_{\max}$ is the largest magnitude event expected. Although other distributions may better describe magnitude–frequency data in detail (Kagan 2002a; Koravos *et al.* 2003), the simpler truncated Gutenberg–Richter (TGR) can often not be rejected by the available data.

We use the data to define a plausible range of a, $b$and $m_{\max}$ combinations. Such combinations should satisfy the following constraints:

(1) The a- and b-values should be compatible with the magnitude–frequency data.

(2) $m_{\max}$ should not greatly exceed $m_{\max}^{\text{cat}}$, the maximum observed event size. The length of the catalogue, T_{cat}, relative to the recurrence interval of $m_{\max}$ events ($T_{\text{rec}}^{\max}$) determines how large a difference between $m_{\max}$ and $m_{\max}^{\text{cat}}$ is plausible. The larger $T_{\text{cat}}/T_{\text{rec}}^{\max}$, the closer $m_{\max}$ and $m_{\max}^{\text{cat}}$ should be.

(3) The combination of a, $b$and $m_{\max}$ should result in a total, long-term, seismic moment rate, $\dot{M}_0^{\text{seis}}$, that is less then or equal to the tectonic moment rate, $\dot{M}_0^{\text{tec}}$, determined geodetically. If $\dot{M}_0^{\text{seis}}$ is less than $\dot{M}_0^{\text{tec}}$, it indicates that part of the deformation is aseismic, which can be expressed in a percentage of aseismic deformation, as a smaller width of the seismogenic zone, or as a coupling factor less than 1.

(4) $\dot{M}_0^{\text{cat}}/\dot{M}_0^{\text{seis}}$ has to be reasonable for the catalogue length relative to $T_{\text{rec}}^{\max}$. If T_{cat} is large, the average catalogue moment rate, $\dot{M}_0^{\text{cat}}$, should be close to the long-term average, $\dot{M}_0^{\text{seis}}$. If however, the catalogue is relatively short, $\dot{M}_0^{\text{cat}}$ can be much smaller, or even larger than $\dot{M}_0^{\text{seis}}$, depending on whether the catalogue happens to include or miss some of the largest events.

Table 2 summarizes the terminology used for the different maximum magnitude and moment rate estimates.

7.1 Source zones

To determine the earthquake recurrence parameters, the study region is divided into 10 areas (Fig. 8), where each area is characterized by a uniform style of deformation. The NAFZ was separated into an eastern section (up to 33 °E), where the strike-slip fault is well-defined (zone 4) and a Marmara Sea section (zone 3), which may contain several splays and accommodates some extension. The diffuse continuation of the NAFZ in the northern Aegean is contained in zone 2. All extension in central Greece and western Anatolia is grouped in zones 6 and 7 respectively. Zone 5 encompasses the Kephalonian strike-slip fault. The active Hellenic Trench is divided into a central section (zone 9), where geodetically measured compression is mainly perpendicular to the trench, and an eastern section (zone 10), where motion is oblique. These two zones may incorporate a small amount of arc-internal deformation, but were drawn to span the dipping interface and allow for larger off-shore earthquake location errors. Zones 1 and 8 contain the low-straining region in northwestern Greece and the southern Aegean respectively. Hazard studies usually define earthquake recurrence parameters within finer source zones. For example, superimposed on Fig. 8 are the source zones of the SESAME seismic hazard project (http://seismo.ethz.ch/gshap/sesame/). However, the density of geodetic and seismic data and location errors of the historical earthquakes do not allow a smaller-scale study. Furthermore, the size of each zone is defined such that the number of events included is large enough to determine statistically significant a- and b-values. Nevertheless, our coarser-grid study provides constraints which earthquake recurrence rates for smaller source zones should satisfy.

7.2 Magnitude–frequency data

Fig. 9 shows the cumulative magnitude–frequency distribution of the two catalogues discussed in Section 4.1. The two data sets show a similar trend. A systematic increase of the cumulative number of earthquakes occurs around $M_{\text{w}} = 6$. Systematic errors in magnitude assignment, in completeness length estimate, missing events with $M_{\text{w}} = 5$–6, or a real increase of the rate of recurrence can explain this change in the distribution with magnitude. Although an increase in recurrence rate may occur in some regions, especially along single faults, it is quite unlikely to occur within all areas and we suspect a systematic catalogue inadequacy to be the cause. In Fig. 9, the grey area delimits the range of magnitude–frequency distributions obtained when random uncertainties in magnitude and completeness length are taken into account. To define this range, magnitudes and completeness intervals are randomly chosen within the uncertainty bounds given in Section 4.1 and in Table 1 yielding 1000 alternative versions of both CAT1 and CAT2. For most of the regions, the uncertainties do not allow us to distinguish a characteristic distribution. Note that the uncertainty ranges in Fig. 9 do not account for possible systematic errors in the catalogues. Koravos *et al.* (2003) did prefer a characteristic distribution for many of their source regions, but it should be noted that the -0.4 magnitude correction they applied tends to enhance characteristic behaviour. Although our data do not unambiguously define a linear trend, we feel they provide

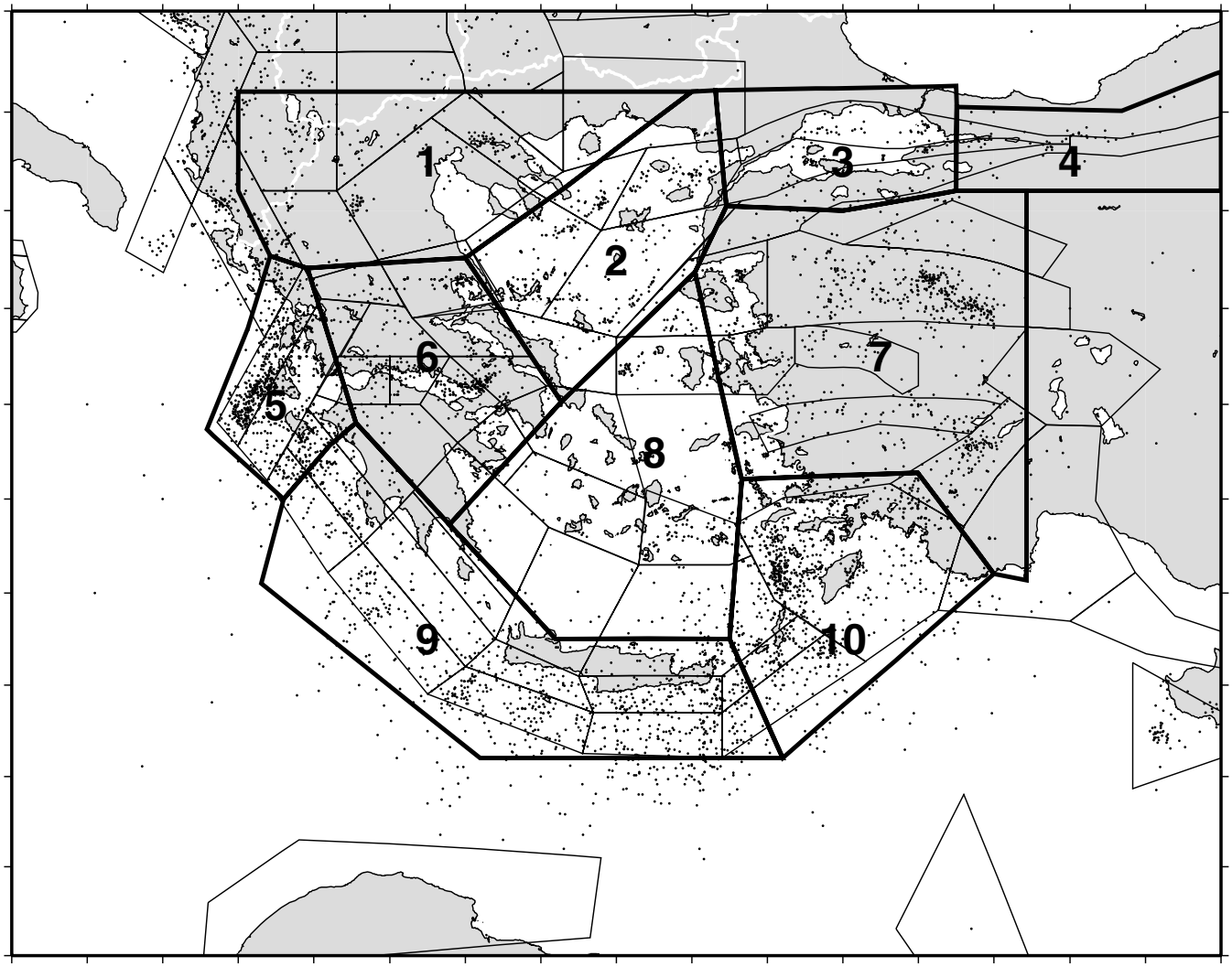

Figure 8. The 10 tectonic areas used to define the earthquake recurrence parameters. Superimposed are the SESAME sources and seismicity (dots) of the historical catalogue CAT1 (Table 1).

insufficient constraints to fit a more complex distribution than the three-parameter truncated Gutenberg–Richter distribution.

7.3 *a*- and *b*-values and m_{max}

As a first step, we determine several end-member a, $b$and m_{max} fits to the magnitude–frequency data. Subsequently, we test how catalogue length affects the possible range of $\dot{M}_0^{cat}/\dot{M}_0^{seis}$. The combinations of a, $b$and m_{max} determined here (Table 3), all assume that $\dot{M}_0^{seis} = \dot{M}_0^{tec}$, that is, they provide an upper bound estimate, m_{max}^{tec}, for m_{max}. The tectonic moment rate $\dot{M}_0^{tec}$ is determined from the geodetic strain rates in Section 6.2, using eq. (3). Assuming homogeneous $\dot{M}_0$ in each small grid cell, $\dot{M}_0^{tec}$ in the 10 larger areas are determined by summing the geodetic moment rates of all grid cells contained in them. If only part of a grid cell overlaps with a seismogenic source zone, the geodetic moment rates are included in proportion to the area intersected.

Some studies (for example Kanamori & Anderson 1975; Wesnousky 1999; Godano & Pingue 2000; Kagan 2002a,b) have argued for a universal b-value of 1. For cases 1 and 2, we fix $b$to 1. a_1 is a maximum a-value obtained by setting m_{max} equal to the minimum possible value m_{max}^{cat}. a_2 is a minimum value, estimated from a maximum-likelihood fit (Aki 1965) to the distribution for events with $M_w = 5$–6, which represents the lower part of the data trend. Note that uncertainties in magnitude are taken into account to estimate the maximum likelihood fit. It is clear from Fig. 9 that $b = 1$ is not always an appropriate value to characterize the frequency–magnitude relationship. For case 3, we find both a_3 and b_3 by a maximum-likelihood fit to CAT1. We find that b_3-values of less than 1 provide a better approximation to the data of the northeastern part of our study region, and b_3-values larger than 1 better approximate the data along the Kephalonian Fault and the Hellenic Trench. This is consistent with results from Papaioannou & Papazachos (2000), who determined a, $b$and m_{max} for smaller Greek source zones. They found b-values systematically increasing from 0.8 in northern Greece to 0.9 in central and southern Greece and southwestern Anatolia, to 1.0 along the Kephalonian Fault and Hellenic Trench. The b_3-values we find in our larger study region range from 0.6 to 1.3.

With the exception of areas 1 and 5, the a_1-curves imply that the historical catalogues underestimate the recurrence rates of all events with $M_w < 6.5$–7. By contrast, the a_2-curve implies, for most areas,

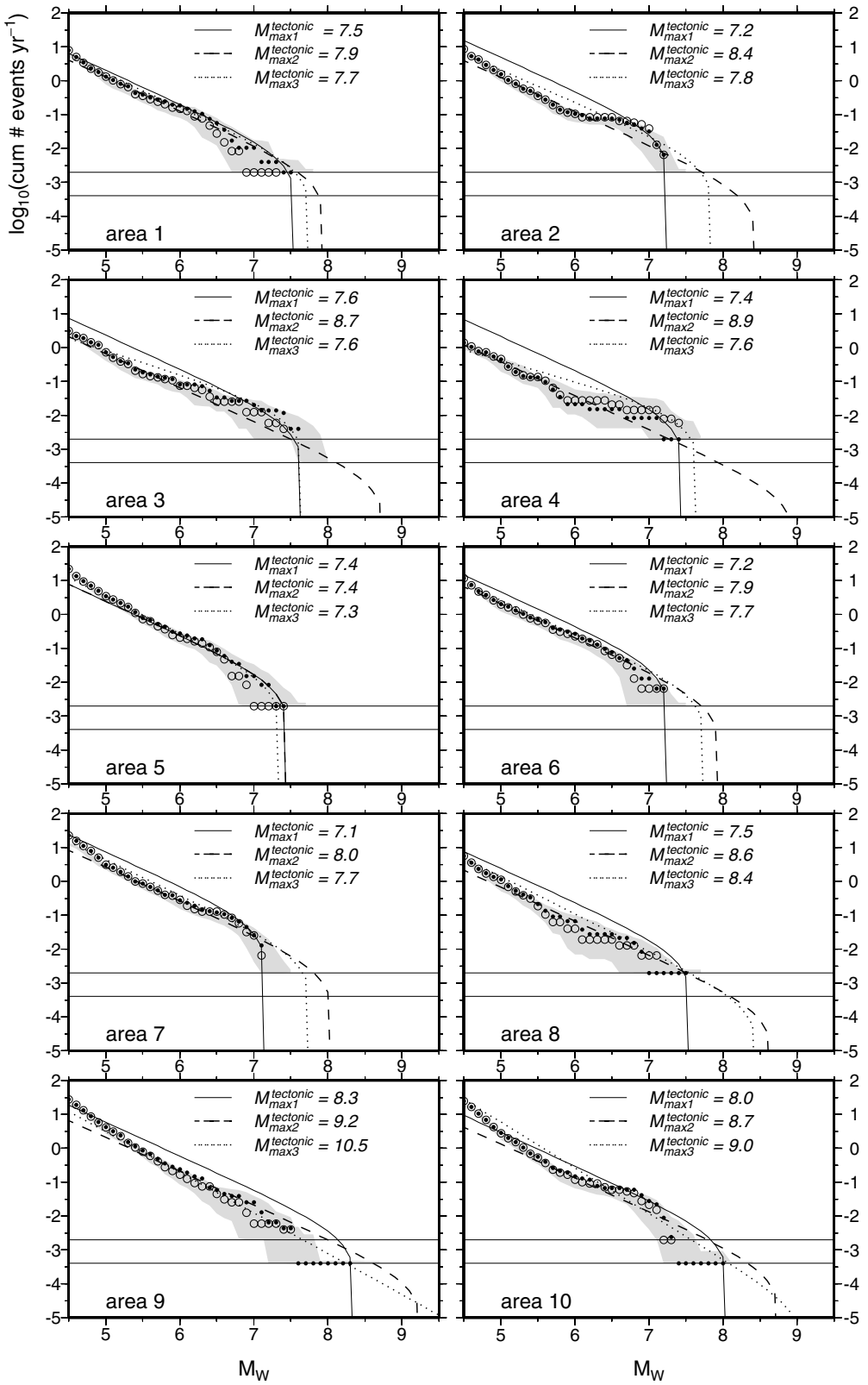

Figure 9. The $\log_{10}$ of the cumulative number of events versus magnitude for the historical seismic catalogues CAT1 (open circles) and CAT2 (filled circles) (Table 1) in each of the areas shown in Fig. 8. The curves represent truncated Gutenberg–Richter approximations to the magnitude–frequency data. The various curves provide an estimate of the range of $m_{\max}^{\text{tec}}$ necessary if all tectonic deformation ($\dot{M}_0^{\text{tec}}$) is accommodated seismically. The different curves are discussed in the text and the parameters are listed in Table 3. Solid lines: $a_1, b_1 = 1, m_{\max}^1$, dashed lines: $a_2, b_2 = 1, m_{\max}^2$, dotted lines: $a_3, b_3, m_{\max}^3$. The two horizontal lines mark the recurrence time equal to the length of the two historical seismic catalogues. The grey area illustrates the uncertainties in the magnitude–frequency data due to non-systematic uncertainties in magnitude and completeness.

Table 3. $\dot{M}_0^{\text{tec}}$ = geodetic (long-term tectonic) moment rate in N m yr^{-1}, a_1 and a_2 resp. a_3 and b_3 are the earthquake recurrence parameters obtained in Section 7.3. b_1 and b_2 are equal to 1 in all areas. $a = \log_{10}$ of the cumulative number of events with $M_w \geq 4$, b = slope of the Gutenberg–Richter relationship, $m_{\max}^{\text{seis}}$ = best estimate of $m_{\max}$, T = recurrence time of $m_{\max}^{\text{seis}}$.

Area no	Area size (100 km^2)	$\dot{M}_0^{\text{tec}}$	a_1	a_2	a_3	b_3	$m_{\max}^{\text{seis}}$	T(yr)
1	714.66	2.88e+18	1.3	1.1	1.2	1.0	7.5–7.7	400–1500
2	522.53	4.95e+18	1.7	1.1	1.2	0.9	7.2–7.7	100–500
3	343.63	3.70e+18	1.3	0.8	0.6	0.7	7.6–7.8	550–1000
4	293.48	2.70e+18	1.3	0.6	0.4	0.6	7.4–7.8	200–1000
5	271.01	3.09e+18	1.4	1.4	1.6	1.1	7.4–7.5	450–500
6	532.57	4.64e+18	1.6	1.3	1.4	1.0	7.2–7.7	100–950
7	1224.46	6.63e+18	1.8	1.4	1.7	1.0	7.2–7.7	100–700
8	904.87	3.39e+18	1.4	0.8	1.2	1.1	7.5–7.8	450–1050
9	1103.10	2.09e+19	1.7	1.3	1.7	1.2	7.5–8.0	350–2500
10	674.25	7.46e+18	1.4	1.1	2.1	1.3	7.5–8.0	400–2500

that the catalogues overestimate the recurrence of events $M_w = 6.5$ –7.5, and that significantly larger events than have been observed can occur. The a_3- and b_3-curves represent the data quite well for the NAFZ areas 3 and 4 with a b-value of 0.7 and 0.6 respectively, and for the Kephalonian Fault (area 5), with a b-value of 1.1. Thus, for these three zones, a reasonable combination of a, $b$and $m_{\max}$ with $\dot{M}_0^{\text{seis}} = \dot{M}_0^{\text{tec}}$ can be found, implying that all deformation is accommodated seismically. A slightly more characteristic distribution for the NAFZ would still give $\dot{M}_0^{\text{seis}} = \dot{M}_0^{\text{tec}}$ for a $m_{\max}^{\text{seis}}$ that does not deviate much from $m_{\max}^{\text{cat}}$. However, the shape of the seismicity distribution in zone 4 may be affected by the poorer data quality east of 30°E. For areas 1, 2, 6 and 7, $m_{\max}^3$ exceeds $m_{\max}^{\text{cat}}$ by only about 0.5 and we cannot reject the possibility that $\dot{M}_0^{\text{seis}} = \dot{M}_0^{\text{tec}}$. In zones 2 and 7, the recurrence times of the missing $M > 7$ events are small enough compared with T_{cat} that a few more events should have been recorded. However, in these two zones, the catalogues may be incomplete. In areas 9 and 10, but also in area 8, $m_{\max}^{2,3}$ are much larger than $m_{\max}^{\text{cat}}$, and larger than we think plausible. In areas 9 and 10, not only the largest events but also other events with $M \geq 7.5$ expected from the curves are absent in the catalogues. This could indicate that a significant part of the motion along the trench occurs aseismically.

7.4 Effect of catalogue length

To assess how much $\dot{M}_0^{\text{cat}}$ might differ from the long-term rate $\dot{M}_0^{\text{seis}}$ (and thereby also $m_{\max}^{\text{cat}}$ from $m_{\max}^{\text{seis}}$), for our catalogue length, we perform a statistical test. As before, we do this for the case that $\dot{M}_0^{\text{seis}} = \dot{M}_0^{\text{tec}}$. Since $m_{\max}^{\text{tec}}$ and its recurrence time are upper estimates, the tests will give the maximum possible range for observed/long-term values.

For a catalogue length $T_{\text{cat}} = 100$, 500 and 2550 yr, 5000 synthetic catalogues each were made from a magnitude–frequency distribution described by a_3, b_3 and $m_{\max}^3$. Events at all magnitudes are assumed to have a Poissonian distribution in time. The synthetic $\dot{M}_0^{\text{cat}}$ define a probability density distribution of the ratio $[\dot{M}_0^{\text{cat}}/\dot{M}_0^{\text{seis}}]$ for a given T_{cat}. Fig. 10 compares the modelled ratios $[\dot{M}_0^{\text{cat}}/\dot{M}_0^{\text{seis}}]_{\text{mod}}$ with the observed ratios $[\dot{M}_0^{\text{cat}}/\dot{M}_0^{\text{tec}}]_{\text{obs}}$. Error ranges for the observed ratios include the factor 2 uncertainty that was estimated by comparing our two catalogues, CAT1 and CAT2, along the NAFZ and within the Marmara Sea where the data in the catalogues differs the most. The much smaller uncertainties in $\dot{M}_0^{\text{tec}}$ are ignored.

In all areas except in areas 8, 9 and 10, the statistical test yields a normal probability distribution of $[\dot{M}_0^{\text{cat}}/\dot{M}_0^{\text{seis}}]_{\text{mod}}$ with a mean value equal to 1 and a small standard deviation (sd) up to 0.08–0.18 (for $T_{\text{cat}} = 100$ yr). In area 8, the large $m_{\max}^3 = 8.4$, which has a recurrence time of about 10 000 yr, yields most likely ratios of $[\dot{M}_0^{\text{cat}}/\dot{M}_0^{\text{seis}}]$ below 1, with a value of 0.6 and 0.9 for a catalogue length of 100 and 500 yr respectively. However, even here, the chance of observing ratios larger than 1 is ≥40 per cent. In areas 9 and 10, where $m_{\max}^3$ (=10.4 and 9 respectively) are larger than we think reasonable, the mean values range between 0.3 and 0.9. But still, for $T_{\text{cat}} = 100$ yr, there is a probability of observing ratios larger than 1 of 15 per cent in zone 9 and 28 per cent in zone 10. Thus, except in areas 9 and 10, the a_3, b_3 seismicity distributions should, even for a 100-yr catalogue, reflect the long-term seismic deformation, and there is an equal likelihood that $\dot{M}_0^{\text{cat}}$ exceeds or underestimates $\dot{M}_0^{\text{seis}}$. Even for the a_3, b_3, $m_{\max}^3$ parameters for areas 9 and 10, the probability that a catalogue of 500 yr or longer reflects long-term seismic deformation is up to 39 per cent.

For the San Andreas Fault in California, which has similarly high strain rates and maximum magnitudes as our study region and a catalogue that covers about 150 yr, $\dot{M}_0^{\text{cat}}$ is comparable to the geodetic moment rate $\dot{M}_0^{\text{tec}}$ (Ward 1998b), that is, geodetic strain is completely released seismically over the time span of the catalogue. By contrast, for the eastern Mediterranean, we find that the short-term catalogue moment rates are always less than the long-term tectonic moment rates ($[\dot{M}_0^{\text{cat}}/\dot{M}_0^{\text{tec}}]_{\text{obs}}$ in Fig. 10), although the statistical tests show that in most areas the probability of $\dot{M}_0^{\text{cat}}$ exceeding or lagging behind $\dot{M}_0^{\text{seis}}$ is equal. There are three possible explanations for the low $[\dot{M}_0^{\text{cat}}/\dot{M}_0^{\text{tec}}]_{\text{obs}}$: (1) the long-term seismic deformation is not equal to the long-term tectonic deformation, that is, a large part of the tectonic deformation is released aseismically; (2) the seismic historical catalogues systematically underestimate the moment rates, that is, the completeness length for one or several magnitude intervals is overestimated; and/or (3) the moment rate over the catalogues happened to be low, that is lacking seismicity will be released in future. Explanation (3) is unlikely to apply to all regions at the same time. We hold a combination of (1) and (2) responsible for the low $[\dot{M}_0^{\text{cat}}/\dot{M}_0^{\text{tec}}]_{\text{obs}}$.

7.5 Estimating long-term seismic deformation $\dot{M}_0^{\text{seis}}$

Based on the results of Section 7.3 and 7.4, we identify three types of areas: (1) regions that have fully seismic deformation, (2) regions that have significant aseismic deformation and (3) regions where the data do not allow us to distinguish between fully seismic and partially aseismic deformation. For a_3 and b_3 we define our best estimates of $m_{\max}^{\text{seis}}$ (Table 3). The corresponding long-term seismic moment rate $\dot{M}_0^{\text{seis}}$ is shown in Fig. 11.

The low seismic moment rates $\dot{M}_0^{\text{cat}}$ and high $m_{\max}^{\text{tec}}$ required are clear evidence for significant aseismic deformation (that is, shallow coupling widths) in the southern Aegean and along the Hellenic Arc

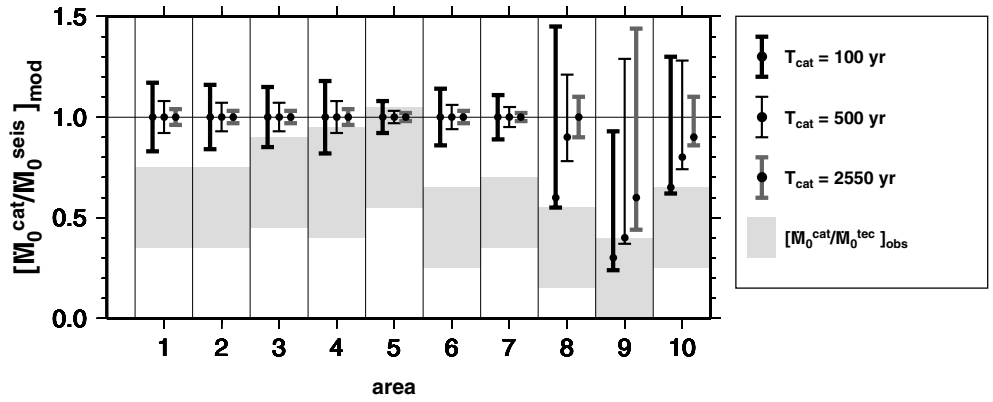

Figure 10. Distribution of ratios $\dot{M}_0^{\rm cat}/\dot{M}_0^{\rm seis}]_{\rm mod}$ obtained for a synthetic catalogue produced using a Poissonian recurrence distribution and a magnitude–frequency distribution characterized by a_3, b_3 and $m^3_{\rm max}$, for a catalogue length of 100 yr (solid line), 500 yr (dotted line) and 2550 yr (grey line). Black dots represent the mean value. Two-thirds of the modelled ratios lie within the error bars. Low $\dot{M}_0^{\rm cat}/\dot{M}_0^{\rm seis}]_{\rm mod}$ are for *a*and *b*implying that a significant part of the strain is released by large infrequent events with recurrence times that are often longer than 2550 yr. In most areas, the observed ratios $\dot{M}_0^{\rm cat}/\dot{M}_0^{\rm tec}]_{\rm obs}$ (in grey) are less than the expected ratios $\dot{M}_0^{\rm cat}/\dot{M}_0^{\rm seis}]_{\rm mod}$.

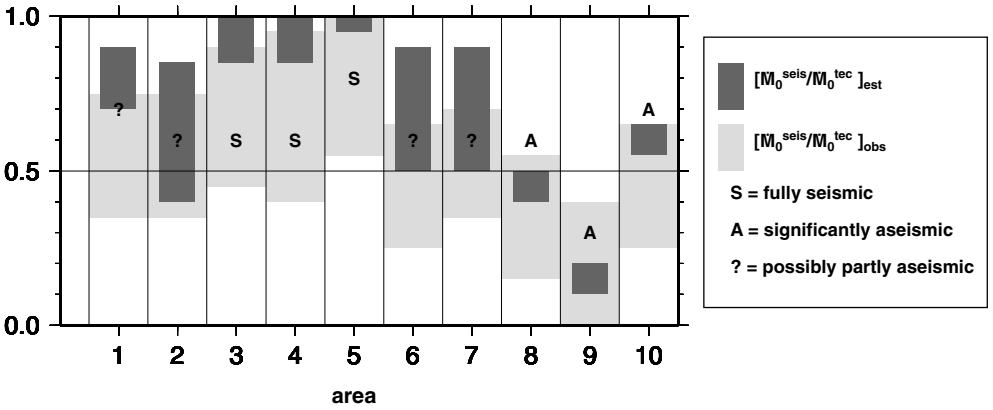

Figure 11. Best estimate and observed moment ratios. $\dot{M}_0^{\rm seis}/\dot{M}_0^{\rm tec}]_{\rm est}$ = ratio of the long-term seismic moment rates and the long-term tectonic moment rates, $\dot{M}_0^{\rm cat}/\dot{M}_0^{\rm tec}]_{\rm obs}$ = ratio of the short-term seismic moment rate and the long-term tectonic moment rates (in dark grey with error intervals in light grey). We distinguish three types of areas: S = areas with fully seismic deformation, A = areas with significant aseismic deformation, ? = areas where the data do not allow us to distinguish between fully seismic and partially aseismic deformation.

in areas 8, 9 and 10. In addition, the largest events in areas 9 and 10 are old and significantly exceed the size of any others recorded in these regions (Fig. 9), leading us to think that even $m^{\rm cat}_{\rm max}$ may be overestimated. For areas 8, 9 and 10 we consider an $m^{\rm seis}_{\rm max}$ between about 7.5 and 8 to be most plausible. This yields $\dot{M}_0^{\rm seis}/\dot{M}_0^{\rm tec} = 40$–50 per cent, <10 per cent, and 55–65 per cent respectively. In area 10, convergence includes an oblique component. The extensional part of this motion is reflected in the focal mechanisms and seems to be responsible for the larger amount of seismic strain. Fully seismic deformation is likely within the Marmara Sea (area 3), along the NAFZ (area 4) and along the Kephalonian Fault (area 5). In Fig. 10, at least one of the estimates of $[\dot{M}_0^{\rm cat}/\dot{M}_0^{\rm tec}]_{\rm obs}$ is close to 1 and $m^3_{\rm max}$ is similar to the observed $m^{\rm cat}_{\rm max}$. $m^{\rm seis}_{\rm max}$ is estimated to be close to $M^3_{\rm max}$: 7.6–7.8 in area 3, 7.4–7.8 in area 4 and 7.4–7.5 in area 5. The corresponding $\dot{M}_0^{\rm seis}$ amounts to 85–100 per cent of $\dot{M}_0^{\rm tec}$ in areas 3 and 4 and 95–100 per cent in area 5. In areas 1, 2, 6 and 7, the data allow a small component of aseismic deformation, especially in zones 2 and 6.

In summary, the strike-slip zones appear to be fully seismic. The trench region is affected by at least 45 per cent aseismic deformation. The other regions are characterized by 10–60 per cent aseismic deformation but uncertainties in the catalogues, in the strain rates and in the assignment of magnitudes do not allow us to be conclusive about this. For most regions, $\dot{M}_0^{\rm tec}$ thus gives a reasonable first-order estimate of $\dot{M}_0^{\rm seis}$, but a catalogue that provides tight constraints for *a*- and *b*-values is necessary for better estimates of the aseismic component of deformation.

8 CONCLUSIONS

In this paper, seismic and geodetic data are combined to estimate earthquake recurrence parameters as used in seismic hazard analyses. We obtain truncated Gutenberg–Richter distribution parameters, *a*-value, *b*-value and $m_{\rm max}$, and the corresponding long-term seismic moment rates $\dot{M}_0^{\rm seis}$, that are consistent with seismicity data, tectonic information and strain rates.

The eastern Mediterranean was chosen as a study region for its dense distribution of data. This density allows for detailed comparison between the short-term seismic strain rate documented by earthquake catalogues and the tectonic strain rate field measured geodetically. For all tectonic regimes, we find that both the seismic strain rate field over several magnitude units and the geodetic strain

rate field are very similar in style. Thus, a catalogue which reflects only the long-term rate of small events can reliably illustrate the deformation style.

The ratio of long-term seismic to total strain is estimated by comparing the amplitudes of the seismic catalogue moment rates $\dot{M}_0^{\rm cat}$ with the geodetic moment rates $\dot{M}_0^{\rm tec}$. Our statistical analyses show that, when averaged over a tectonic regime, the moment rates contained in the historical catalogues should estimate (within 10–25 per cent) the long-term seismic moment rate well. It is as likely that an $\dot{M}_0^{\rm cat}$ that exceeds $\dot{M}_0^{\rm seis}$ will be observed as one that lags behind it. This applies generally to areas like the eastern Mediterranean and California where strain rates are of the order of 100 nanostrain (1 nanostrain $= 10^{-9}$ yr^{-1}), $m_{\rm max}$ does not exceed 8–8.5 and the catalogue spans at least 100–200 yr. In the eastern Mediterranean, however, the observed $\dot{M}_0^{\rm cat}$ is systematically lower than $\dot{M}_0^{\rm tec}$. Errors in magnitude or catalogue completeness estimates probably contribute to these low $\dot{M}_0^{\rm cat}$ estimates. Good constraints are also important for small earthquakes since for *b*-values larger than or equal to 1 events with $M_{\rm w} = 4.5$–6.5 can accommodate up to 60 per cent of the deformation.

From the very large maximum magnitudes required to accommodate the geodetically observed strain along the Hellenic Arc, we infer that less than 55 per cent of the convergence occurs seismically, consistent with previous results (Main & Burton 1989; Koravos *et al.* 2003). This implies that the trench is largely uncoupled, as has been observed for other trenches with backarc spreading and/or retreating downgoing plates (Scholz & Campos 1995). In contrast, the strike-slip zones encompassing the NAFZ and the Kephalonian Fault are fully seismic. A small component of aseismic deformation may characterize the prolongation of the NAFZ into the Northern Aegean Trough (NAT). This aseismic component may be due to the relative immaturity of the plate boundary here. For the extensional zones in central and northern Greece and western Turkey, up to 10–60 per cent of the deformation is aseismic. In the southern Aegean, deformation occurs mostly aseismically. Very thin lithosphere due to extension and hydration by the subducting slab probably limits the seismogenic thickness.

Averaged over tectonic zones, $\dot{M}_0^{\rm cat}$ should approach $\dot{M}_0^{\rm seis}$. However, on a smaller scale, the seismic strain rate field inferred from the catalogues (Fig. 6) is rougher than the long-term tectonic strain rate field (Fig. 7). This variability in short-term seismic strain rate field reflects that the largest events lead to deficits or excesses of seismic moment release. For example, along the NAFZ a local lack of seismicity is found in the Marmara Sea. However, when moment rates are averaged over a region also including the strike-slip faults south of the Marmara Sea there is no clear deficiency of seismic strain release in the last 500 yr.

ACKNOWLEDGMENTS

We thank Bill Holt and John Haines for making the strain rate mapping programme available and Corné Kreemer for his help with the implementation of the method. We thank James Jackson for providing his catalogue. This project benefited from discussions with Steven Ward and David Jackson. We also thank the latter for providing a solution to include magnitude uncertainties in the maximum likelihood approach. The SESAME data were obtained from Maria-Jose Jimenez (IGCP no 382 project). We are also grateful to John Beavan, Corné Kreemer and an anonymous reviewer for their thoughtful reviews of the manuscript. This research was funded by MunichRe and ETH Zurich. This is contribution no 1248 of the Institute of Geophysics, ETH Zurich.

REFERENCES

Abe, K. & Noguchi, S., 1983. Revision of magnitudes of large shallow earthquakes, 1897–1912, *Phys. Earth planet. Int.,* **33,** 1–11.

Aki, K., 1965. Maximum likelihood estimate of the parameter b in the formula log $N = a - bm$ and its confidence limits, *Bull. Earthquake Res. Inst. Tokyo Uni.,* **43,** 237–239.

Ambraseys, N.N., 2001a. Reassessment of earthquakes, 1900–1999, in the Eastern Mediterranean and the Middle East, *Geophys. J. Int.,* **145,** 471–485.

Ambraseys, N.N., 2001b. The Kresna earthquake of 1904 in Bulgaria, *Ann. Geofis.,* **44,** 95–117.

Ambraseys, N.N. & Jackson, J.A., 2000. Seismicity of the Sea of Marmara Turkey since 1500, *Geophys. J. Int.,* **141,** F1–F6.

Amelung, F. & King, G., 1997. Large-scale tectonic deformation inferred from small earthquakes, *Nature,* **386,** 702–705.

Anderson, H. & Jackson, J.A., 1987. Active tectonics of the Adriatic region, *Geophys. J. R. astr. Soc.,* **91,** 937–983.

Argus, D.F. & Heflin, M.B., 1995. Plate motion and crustal deformation estimated with geodetic data from GPS, *Geophys. Res. Lett.,* **22**(15), 1973–1976.

Armijo, R., Lyon-Caen, H. & Papanastassiou, D., 1992. E–W extension and Holocene normal-fault scarps in the Hellenic arc, *Geology,* **20,** 491–494.

Armijo, R., Hubert, A. & Barka, A., 1999. Westward propagation of the North Anatolian Fault into the northern Aegean: timing and kinematics, *Geology,* **27**(3), 267–270.

Barka, A., 1992. The North Anatolian Fault Zone, *Ann. Tecton.,* **VI**(Suppl.), 164–195.

Barka, A., 1997. Neotectonics of the Marmara Sea region, in *Active Tectonics of Northwestern Anatolia—The MARMARA Poly-Project*, pp. 55–88, eds Schindler, C. & Pfister, M., VdF Hochschulverlag AG, ETH Zürich.

Barka, A. & Kandinsky-Cade, K., 1988. Strike-slip fault geometry in Turkey and its influence on earthquake activity, *Tectonics,* **7**(3), 663–684.

Beavan, J. & Haines, J., 2001. Contemporary horizontal velocity and strain rate fields of the Pacific-Australian plate boundary zone through New Zealand, *J. geophys. Res.,* **106,** 741–770.

Clarke, P. *et al.,* 1998. Crustal strain in Central Greece from repeated GPS measurements in the interval 1989–1997, *Geophys. J. Int.,* **134**(4), 195–214.

Cocard, M., Kahle, H.-G., Peter, Y., Geiger, A., Veis, G., Felekis, S., Billiris, H. & Paradissis, D., 1999. New constraints on the rapid crustal motion of the Aegean region: recent results inferred from GPS measurements (1993–1998) across the West Hellenic Arc, Greece, *Earth planet. Sci. Lett.,* **172,** 39–47.

Davies, R., England, P., Parsons, B., Billiris, H., Paradissis, D. & Veis, G., 1997. Geodetic strain of Greece in the interval 1892–1992, *J. geophys. Res.,* **102,** 24 571–24 588.

DeMets, C., Gordon, R., Argus, D. & Stein, S., 1994. Current plate motions, *Geophys. J. Int.,* **101,** 425–478.

Dziewonski, A., Chou, T.-A. & Woodhouse, J., 1981. Determination of earthquake source parameters from waveform data for studies of global and regional seismicity, *J. geophys. Res.,* **86,** 2825–2852.

Eyidoğan, H., 1988. Rates of crustal deformation in western Turkey as deduced from major earthquakes, *Tectonophysics,* **148,** 83–92.

Fernandes, R.M.S., Ambrosius, B.A.C., Noomen, R., Bastos, L., Wortel, M.J.R., Spakman, W. & Govers, R., 2003. The relative motion between Africa and Eurasia as derived from ITRF2000 and GPS data, *Geophys. Res. Lett.,* **30**(16), doi:10.1029/2003GL017089.

Field, E.H., Johnson, D.D. & Dolan, J.F., 1999. A mutually consistent seismic-hazard source model for Southern California, *Bull. seism. Soc. Am.,* **89**(3), 559–578.

Gautier, P., Brun, J.P., Moriceau, R., Sokoutis, D., Martinod, J. & Jolivet, L., 1999. Timing, kinematics and cause of Aegean extension a scenario based on a comparison with simple analogue experiments, *Tectonophysics,* **315,** 31–72.

Giardini, D., 1999. The Global Seismic Hazard Assessment Program (GSHAP) 1992–1999, *Ann. Geofis.,* **42**(6), 957–974.

Giardini, D. & Basham, P., 1993. The Global Seismic Hazard Assessment Program (GSHAP), *Ann. Geofis.,* **36**(3–4), 3–13.

Giunchi, C., Kiratzi, A., Sabadini, R. & Louvari, E., 1996. A numerical model of the Hellenic subduction zone: active stress field and sea-level changes, *Geophys. Res. Lett.,* **23**(18), 2485–2488.

Godano, C. & Pingue, F., 2000. Is the seismic moment-frequency relation universal?, *Geophys. J. Int.,* **142,** 193–198.

Haines, A.J. & Holt, W.E., 1993. A procedure for obtaining the complete horizontal motions within zones of distributed deformation from the inversion of strain rate data, *J. geophys. Res.,* **98,** 12 057–12 082.

Haines, A.J., Jackson, J.A., Holt, W.E. & Agnew, D.C., 1998. Representing distributed deformation by continuous velocity fields, in *Science Report 98/5*, Institute of Geological and Nuclear Science, Wellington, New Zealand.

Hanks, T. & Kanamori, H., 1979. A moment magnitude scale, *J. geophys. Res.,* **84,** 2348–2350.

Hatzfeld, D., Ziazia, M., Kementzetzidou, D., Hatzidimitriou, P., Panagiotopoulos, D., Makropoulos, K., Papadimitriou, P. & Deschamps, A., 1999. Microseismicity and focal mechanisms at the western termination of the North Anatolian Fault and their implications for continental tectonics, *Geophys. J. Int.,* **137**(3), 891–908.

Hollenstein, C., Kahle, H.-G., Geiger, A., Jenny, S., Goes, S. & Giardini, D., 2003. New GPS constraints on the Africa–Eurasia plate boundary zone in southern Italy, *Geophys. Res. Lett.*, **30**(18), 1935, doi: 10.1029/2003GL017554

Holt, W.E. & Haines, A.J., 1995. The kinematics of northern South Island, New Zealand, determined from geologic strain rates, *J. geophys. Res.,* **100,** 17 991–18 010.

Jackson, J.A. & McKenzie, D.P., 1984. Active tectonics of the Alpine-Himalayan belt between western Turkey and Pakistan, *Geophys. J. R. astr. Soc.,* **77,** 185–264.

Jackson, J.A. & McKenzie, D.P., 1988. The relationship between plate motions and seismic moment tensors, and the rates of active deformation in the Mediterranean and Middle East, *Geophys. J. R. astr. Soc.,* **93,** 45–73.

Jackson, J.A., Haines, J. & Holt, W., 1992. The horizontal velocity field in the deforming Aegean Sea region determined from the moment tensors of earthquakes, *J. geophys. Res.,* **97**(B12), 17 657–17 683.

Jackson, J.A., Haines, J. & Holt, W., 1994. A comparison of satellite laser ranging and seismicity data in the Aegean region, *Geophys. Res. Lett.,* **21**(25), 2849–2852.

Jolivet, L., 2001. A comparison of geodetic and finite strain pattern in the Aegean, geodynamic implications, *Earth planet. Sci. Lett.,* **187,** 95–104.

Jolivet, L., Brun, J., Gautier, P., Lallemant, S. & Patriat, M., 1994. 3D kinematics of extension in the Aegean region from the early Miocene to the present, insights from the ductile crust, *Bull. Soc. géol. France,* **165**(3), 195–209.

Kagan, Y.Y., 2002a. Seismic moment distribution revisited: I. Statistical results,, *Geophys. J. Int.,* **148,** 520–541.

Kagan, Y.Y., 2002b. Seismic moment distribution revisited: II. Moment conservation principle, *Geophys. J. Int.,* **149,** 731–754.

Kahle, H.-G., Müller, M.V. & Veis, G., 1996. Trajectories of crustal deformation of western Greece from GPS observations 1989–1994, *Geophys. Res. Lett.,* **23**(6), 677–680.

Kahle, H.-G. *et al.,* 1999. The GPS strain rate field in the Aegean Sea and western Anatolia, *Geophys. Res. Lett.,* **26**(16), 2513–2516.

Kahle, H.-G., Cocard, M., Peter, Y., Geiger, A., Reilinger, R., Barka, A. & Veis, G., 2000. GPS-derived strain rate field within the boundary zones of the Eurasian, African, and Arabian Plates, *J. geophys. Res.,* **105,** 23 353–23 370.

Kanamori, H. & Anderson, D.L., 1975. Theoretical basis of some empirical relations in seismology, *Bull. seism. Soc. Am.,* **65,** 1073–1096.

King, G., Sturdy, D. & Whitney, J., 1993. The landscape geometry and active tectonics of northwestern Greece, *Geol. Soc. Am. Bull.,* **105,** 137–161.

Kiratzi, A.A., 1993. Study on the active crustal deformation of the North and East Anatolian Fault zones, *Tectonophysics,* **225,** 191–203.

Koravos, G.C., Main, I.G., Tsapanos, T.M. & Musson, R.M.W., 2003. Maximum earthquake magnitudes in the Aegean area constrained by tectonic moment release rates, *Geophys. J. Int.,* **152,** 94–112.

Kostrov, V.V., 1974. Seismic moment and energy of earthquakes, and seismic flow of rocks, *Izv. Acad. Sci. USSR Phys. Solid Earth,* **1,** 23–44, Engl. Trans.

Kotzev, V., Nakov, R., Burchfiel, B., King, R. & Reilinger, R., 2001. GPS study of active tectonics in Bulgaria: results from 1996 to 1998, *J. Geodyn.,* **31,** 189–200.

Kreemer, C. & Chamot-Rooke, N., 2004. Contemporary kinematics of the Southern Aegean and the Mediterranean Ridge, *Geophys. J. Int.* In Press.

Kreemer, C., Holt, W.E., Goes, S. & Govers, R., 2000. Active deformation in the eastern Indonesia and Philippines from GPS and seismicity data, *J. geophys. Res.,* **105,** 663–680.

Kreemer, C., Holt, W.E. & Haines, J.A., 2003. An integrated global model of present-day plate motions and plate boundary deformation, *Geophys. J. Int.,* **154,** 8–34.

Le Pichon, X. & Angelier, J., 1979. The Hellenic Arc and Trench system: a key to the neotectonic evolution of the Eastern Mediterranean area, *Tectonophysics,* **60,** 1–42.

Le Pichon, X., Chamot-Rook, N., Lallemant, S., Noomen, R. & Veis, G., 1995. Geodetic determination of the kinematics of Central Greece with respect to Europe: implication for eastern Mediterranean tectonics, *J. geophys. Res.,* **100**(B7), 12 675–12 690.

Louvari, E., Kiratzi, A.A. & Papazachos, B.C., 1999. The Cephalonia transform fault and its extension to western Lefkada island (Greece), *Tectonophysics,* **308,** 223–226.

Lyberis, N., Yurur, T., Chorowicz, J., Kasapoglu, E. & Gundogdu, N., 1992. The East Anatolian fault: an oblique collisional belt, *Tectonophysics,* **204,** 1–15.

Lyon-Caen, H. *et al.,* 1988. The 1986 Kalamata (South Peloponessus) earthquake: detailed study of a normal fault, evidences for east-west extension in the Hellenic arc, *J. geophys. Res.,* **93,** 14 967–15 000.

Main, I.G. & Burton, P.W., 1989. Seismotectonics and the earthquake frequency magnitude distribution in the Aegean area, *Geophys. J. Int.,* **98**(3), 575–586.

Makris, J., 1978. Some geophysical consideration on the geodynamic situation in Greece, *Tectonophysics,* **46,** 251–268.

Mantovani, E., Viti, M., Albarello, D., Tamburelli, C., Babbucci, D. & Cenni, N., 2000. Role of kinematically induced horizontal forces in Mediterranean tectonics: insights from numerical modeling, *J. Geodyn.,* **30**(3), 287–320.

McClusky, S. *et al.,* 2000. Global Positioning System constraints on plate kinematics and dynamics in the eastern Mediterranean and Caucasus, *J. geophys. Res.,* **105,** 5696–5719.

McKenzie, D.P., 1978. Active tectonics of the Alpine-Himalayan belt: the Aegean Sea and surrounding regions, *Geophys. J. R. astr. Soc.,* **55,** 217–254.

Meijer, P. & Wortel, M., 1997. Present-day dynamics of the Aegean region: a model analysis of the horizontal pattern of stress and deformation, *Tectonics,* **16**(6), 879–895.

Mulargia, F., Gasperini, P. & Tinti, S., 1987. Contour mapping of Italian seismicity, *Tectonophysics,* **142,** 203–216.

Nyst, M. C.J., 2001. A new approach to model the kinematics of crustal deformation with applications to the Aegean and Southeast Asia, *PhD thesis*, Delft University of Technology, The Netherlands.

Papaioannou, C. & Papazachos, B., 2000. Time-independent and time-dependent seismic hazard in Greece based on seismogenic sources, *Bull. seism. Soc. Am.,* **90,** 22–33.

Papazachos, B.C., Kiratzi, A.A. & Karacostas, B.G., 1997. Toward a homogeneous moment-magnitude determination for earthquakes in Greece and the surrounding area, *Bull. seism. Soc. Am.,* **87**(2), 474–483.

Papazachos, B.C., Comninakis, P.E., Karakaisis, G.F., Karakostas, B.G., Papaioannou, C.A., Papazachos, C.B. & Scordilis, E.M., 2000. A catalogue of earthquakes in Greece and surrounding area for the period 550BC-1999, in *International Handbook of Earthquake and Engineering Seismology*, International Association of the Seismology and Physics of the Earth's Interior, Academic Press, Amsterdam.

Papazachos, B.C., Karakostas, V.G., Kiratzi, A.A., Margaris, B.N., Papazachos, C.B. & Scordilis, E.M., 2002. Uncertainties in the estimation of earthquake magnitudes in Greece, *J. Seismol.,* **6,** 557–570.

Papazachos, C.B., 1999. An alternative method for a reliable estimation of seismicity with an application in Greece and the surrounding area, *Bull. seism. Soc. Am.,* **89**.

Papazachos, C.B. & Kiratzi, A., 1992. A formulation for reliable estimation of active crustal deformation and its application to Central Greece, *Geophys. J. Int.,* **111,** 424–432.

Reilinger, R.E. *et al.,* 1997. Global Positioning System measurements of present-day crustal movements in the Arabia-Africa-Eurasia plate collision zone, *J. geophys. Res.,* **102**(B5), 9983–9999.

Robertson, A. & Shallo, M., 2000. Mesozoic-Tertiary tectonic evolution of Albania in its regional Eastern Mediterranean context, *Tectonophysics,* **316,** 197–254.

Savage, J.C. & Simpson, R.W., 1997. Surface strain accumulation and the seismic moment tensor, *Bull. seism. Soc. Am.,* **87,** 1345–1353.

Scholz, C.H. & Campos, J., 1995. On the mechanism of seismic decoupling and back arc spreading at subduction zones, *J. geophys. Res.,* **100**(B11), 22 103–22 115.

Sella, G.F., Dixon, T.H. & Mao, A.L., 2002. REVEL: a model for Recent plate velocities from space geodesy, *J. geophys. Res.,* **107**(B4), 2081.

Seyitoglu, G. & Scott, B.C., 1996. The cause of N–S extensional tectonics in western Turkey: tectonic escape vs back-arc spreading vs orogenic collapse, *J. Geodyn.,* **22,** 145–153.

Shen-Tu, B., Holt, W.E. & Haines, A.J., 1999. Deformation kinematics in the western United States determined from Quaternary fault slip rates and recent geodetic data, *J. geophys. Res.,* **104,** 28 927–28 955.

Sorel, D., 2000. A Pleistocene and still-active detachment fault and the origin of the Corinth-Patras rift, Greece, *Geology,* **28**(1), 83–86.

Straub, C., Kahle, H.-G. & Schindler, C., 1997. GPS and geologic estimates of the tectonic activity in the Marmara Sea region, NW Anatolia, *J. geophys. Res.,* **102**(B12), 27 587–27 601.

Taymaz, T., Eyidogan, H. & Jackson, J., 1991a. Source parameters of large earthquakes in the East Anatolian fault zone, *Geophys. J. Int.,* **106,** 537–550.

Taymaz, T., Jackson, J. & McKenzie, D., 1991b. Active tectonics of the north and central Aegean Sea, *Geophys. J. Int.,* **106,** 433–490.

US Geological Survey, 1998. *Preliminary Determination of Earthquakes (PDE), Monthly Listings*, US Department of the Interior, National Earthquake Information Center, Denver, CO.

Ward, S.N., 1990. Pacific-North America plate motions: new results from very long baseline interferometry, *J. geophys. Res.,* **95,** 21 965–21 981.

Ward, S.N., 1998a. On the consistency of earthquake moment release and space geodetic strain rates: Europe, *Geophys. J. Int.,* **135,** 1011–1018.

Ward, S.N., 1998b. On the consistency of earthquake moment rates, geological fault data, and space geodetic strain: the United States, *Geophys. J. Int.,* **134,** 172–186.

Wesnousky, S.G., 1999. Crustal deformation processes and the stability of the Gutenberg–Richter relationship, *Bull. seism. Soc. Am.,* **89**(4), 1131–1137.

Westaway, R., 1990. Seismicity and tectonic deformation rate in Soviet Armenia: implications for local earthquake hazard and evolution of adjacent regions, *Tectonics,* **9,** 477–503.

Westaway, R., 1994. Present-day kinematics of the Middle East and eastern Mediterranean, *J. geophys. Res.,* **99**(6), 12 071–12 090.